Title	An Unexpectedly Low-redshift Excess of Swift Gamma-ray Burst Rate
Author(s)	Yu, H; Wang, FY; Dai, ZG; Cheng, KS
Citation	The Astrophysical Journal Supplement Series, 2015, v. 218 n. 1, article no. 13
Issued Date	2015
URL	http://hdl.handle.net/10722/214462
Rights	This work is licensed under a Creative Commons Attribution-NonCommercial-NoDerivatives 4.0 International License.

An unexpectedly low-redshift excess of *Swift* gamma-ray burst rate

H. Yu[1], F. Y. Wang[1,2,3]*, Z. G. Dai[1,2] and K. S. Cheng[3]

[1] *School of Astronomy and Space Science, Nanjing University, Nanjing 210093, China*
[2] *Key Laboratory of Modern Astronomy and Astrophysics (Nanjing University), Ministry of Education, Nanjing 210093, China*
[3] *Department of Physics, University of Hong Kong, Pokfulam Road, Hong Kong, China*

*fayinwang@nju.edu.cn

ABSTRACT

Gamma-ray bursts (GRBs) are the most violent explosions in the Universe and can be used to explore the properties of high-redshift universe. It is believed that the long GRBs are associated with the deaths of massive stars. So it is possible to use GRBs to investigate the star formation rate (SFR). In this paper, we use Lynden-Bell's c^- method to study the luminosity function and rate of *Swift* long GRBs without any assumptions. We find that the luminosity of GRBs evolves with redshift as $L(z) \propto g(z) = (1+z)^k$ with $k = 2.43^{+0.41}_{-0.38}$. After correcting the redshift evolution through $L_0(z) = L(z)/g(z)$, the luminosity function can be expressed as $\psi(L_0) \propto L_0^{-0.14\pm0.02}$ for dim GRBs and $\psi(L_0) \propto L_0^{-0.70\pm0.03}$ for bright GRBs, with the break point $L_0^b = 1.43\times10^{51}$ erg s^{-1}. We also find that the formation rate of GRBs is almost constant at $z < 1.0$ for the first time, which is remarkably different from the SFR. At $z > 1.0$, the formation rate of GRB is consistent with the SFR. Our results are dramatically different from previous studies. Some possible reasons for this low-redshift excess are discussed. We also test the robustness of our results with Monte Carlo simulations. The distributions of mock data (i.e., luminosity-redshift distribution, luminosity function, cumulative distribution and $\log N - \log S$ distribution) are in good agreement with the observations. Besides, we also find that there are remarkable difference between the mock data and the observations if long GRB are unbiased tracers of SFR at $z < 1.0$.

Subject headings: gamma-ray burst: general - stars: formation - stars: luminosity function

1. Introduction

Gamma-ray bursts (GRBs) are a kind of the most violent explosions in the Universe, which radiate huge energy in gamma-ray in a short time (for reviews, see Mészáros 2006; Zhang 2007; Gehrels et al. 2009). They are so bright and can be detected at much higher redshifts than supernovae (SNe). Hitherto, the farthest GRB with spectroscopic redshift is GRB 090423 at $z \approx 8.2$ (Tanvir et al. 2009; Salvaterra et al. 2009a). So GRBs may be useful tools to probe the early universe (Bromm & Loeb 2012; Wang et al. 2014), including dark energy (Dai et al. 2004; Schaefer 2007; Wang et al. 2011), star formation rate (Totani 1997; Wang 2013), reionization (Totani et al. 2006; McQuinn et al. 2008), and metal enrichment (Wang et al. 2012; Castro-Tirado et al. 2013).

Theoretically, the progenitors of long GRBs with duration time $T_{90} > 2$ s are thought to be collapse of massive stars (Woosley 1993). Observations also show that some long GRBs are associated with the deaths of massive stars which will give core collapse supernovae (Stanek et al. 2003; Hjorth et al. 2003). So GRBs can be used to investigate the star formation rate (SFR) at high redshifts (Totani 1997; Wijers et al. 1998; Lamb & Reichart 2000; Porciani & Madau 2001; Bromm & Loeb 2002; Lin et al. 2004; Kistler et al. 2009; Wang & Dai 2009; Wanderman & Piran 2010; Butler et al. 2010; Elliott et al. 2012, 2014). In order to measure SFR by using GRBs, the relation between the rate of GRBs and SFR should be known. Some studies found that the GRB rate is consistent with SFR at about $z < 4.0$, but has an excess at high redshift comparing with that expected from SFR (Le & Dermer 2007; Kistler et al. 2009). Some models have been proposed to explain the discrepancy between SFR and GRB rate, such as the cosmic metallicity evolution (Li 2008; Qin et al. 2010), superconducting cosmic strings (Cheng et al. 2010), evolving initial mass function (IMF) of stars (Wang & Dai 2011), evolution of the GRB luminosity function break (Virgili et al. 2011). From the redshift distribution of GRBs and the metallicity of GRB host galaxies, Wang & Dai (2014) showed that the discrepancy between the GRB rate and SFR can be reconciled by considering that GRBs occur in low-metallicity galaxies.

In previous literatures, the $\log N - \log P$ distribution has been used to study the luminosity function and formation rate of GRBs (Fenimore & Ramire Ruiz 2000; Firmani et al. 2004; Guetta et al. 2005; Guetta & Piran 2007; Salvaterra & Chincarini 2007; Salvaterra et al. 2009b; Cao et al. 2011). But the $\log N - \log P$ distribution is the production of the intrinsic luminosity function convolving with the formation rate of GRBs, so the luminosity function and formation rate of GRBs are degenerated (Firmani et al. 2004; Guetta & Piran 2007; Howell et al. 2014).

Moreover, there are several selection effects on the observed redshift distribution of GRBs (Coward 2007), and so the rate of GRBs. The most important one is the observa-

tional limit of satellite. The *Swift* satellite has a flux limit, which means that it can not detect GRB dimmer than the flux limit. So the observed data is truncated, it will be difficult to get the intrinsic distribution of GRB before the selection effect is corrected. Lynden Bell (1971) applied a novel method to study the luminosity function and density evolution from flux-limit quasar sample, which is called Lynden-Bell's c^- method (Lynden-Bell 1971). After that, this method has been widely used in some other objects, such as galaxies (Kirshner et al. 1978; Merighi et al. 1986; Peterson et al. 1986; Loh & Spillar 1986), long GRBs (Yonetoku et al. 2004; Lloyd-Ronning et al. 2002; Kocevski & Liang 2006; Wu et al. 2012), and short GRBs (Yonetoku et al. 2014). The basis of Lynden-Bell's c^- method is that the distributions of luminosity L and redshift z are independent (Lynden-Bell 1971; Efron & Petrosian 1992). So before applying this method, we need to test the independence of L and z with a non-parametric test method provided by Efron & Petrosian (1992). Lynden-Bell's c^- method is a powerful method to estimate the luminosity function and formation rate of objects with truncated sample. For example, Yonetoku et al. (2004) used this method to derive the luminosity function and the formation rate of GRB from 689 *BATSE* GRBs with pseudo redshifts. They found that the GRB formation rate increases quickly at $0 < z < 1$, and remains approximately constant up to $z \sim 10$, which is consistent with observed SFR at $z < 4.0$. Kocevski & Liang (2006) found that the GRB comoving rate density rises steeply at $z < 1.0$, followed by flattening and declines at about $z > 3.0$. Wu et al. (2012) also studied the formation rate of 95 *Swift* GRBs using Lynden-Bell's c^- method, and found that the GRB formation rate increases quickly at $0 < z < 1.0$, and remains approximately constant at $1.0 < z < 4.0$, but finally decreases at $z > 4.0$, which is well consistent with the SFR (Hopkins & Beacon 2006; Kistler et al. 2009; Yüksel et al. 2008; Wang & Dai 2009).

In this paper, we study luminosity function and formation rate of latest *Swift* GRBs by using Lynden-Bell's c^- method. The Lynden-Bell's c^- method can break the degeneracy between luminosity function and GRB formation rate. This paper is organized as follows. We introduce the data from *Swift* satellite, and make the K-correction in the next section. The introductions to Lynden-Bell's c^- method and the nonparametric τ statistical method are given in section 3. In section 4, we derive the luminosity function and formation rate of GRBs. Monte Carlo simulation is used to test our results in section 5. Finally, section 6 presents conclusions and discussions. Throughout the paper, we assume a flat ΛCDM universe with $\Omega_m = 0.27$ and $H_0 = 70$ km s^{-1}Mpc^{-1}.

2. GRB sample

Swift is a multi-wavelength satellite to observe GRBs. It has instruments designed to analyze the bursts, X-ray and UV/optical afterglows, which can locate the positions of GRBs. We collect 127 long GRBs with well measured spectral parameters given by *Fermi-GBM* and *Konus-wind*. These GRBs have redshift data observed by *Swift*. In Table 1, we list the GRB sample, including name (Column 1), redshift (Column 2), low-energy power-law index α (Column 3), high-energy power-law index β (Column 4), peak energy of the νF_ν spectrum in observer's frame (Column 5), peak flux in a certain energy range (Column 6), energy range (Column 7), bolometric luminosity (Column 8) and references (Column 9) of GRBs.

Two spectral models are used to fit the spectra of GRBs, including a power law with an exponential cutoff model (PLEXP) and the Band model (Band et al. 1993). The functional forms are as follows,

$$f(E) = A(\frac{E}{100\ \mathrm{keV}})^{\alpha} \exp^{-\frac{(2+\alpha)E}{E_\mathrm{p}}}, \tag{1}$$

$$f(E) = \begin{cases} A(\frac{E}{100\ \mathrm{keV}})^{\alpha} \exp -\frac{(2+\alpha)E}{E_\mathrm{p}} & E < \frac{(\alpha-\beta)E_\mathrm{p}}{2+\alpha}, \\ A(\frac{E}{100\ \mathrm{keV}})^{\beta} \exp^{\beta-\alpha}(\frac{(\alpha-\beta)E_\mathrm{p}}{(2+\alpha)100\ \mathrm{keV}})^{\alpha-\beta} & E \geq \frac{(\alpha-\beta)E_\mathrm{p}}{2+\alpha}, \end{cases} \tag{2}$$

which represent a power law with an exponential cutoff model and the Band model respectively.

Because the peak fluxes are observed in a lager range of redshifts which correspond to different range of energy bands in the rest frame of GRBs. The K-correction is required to get the bolometric luminosity of GRBs (Bloom et al. 2001). The bolometric luminosity of GRB is

$$L = 4\pi d_L^2(z) F K, \tag{3}$$

where

$$d_L(z) = \frac{c}{H_0} \int_0^z \frac{dz}{\sqrt{1-\Omega_m+\Omega_m(1+z)^3}} \tag{4}$$

is the luminosity distance at redshift z, F is the peak flux observed between between a certain energy range (E_{min}, E_{max}), and the K is the factor of K-correction. If the flux F is in units of erg cm^{-2} s^{-1}, the parameter K is defined as

$$K = \frac{\int_{1\mathrm{keV}/(1+z)}^{10^4\mathrm{keV}/(1+z)} Ef(E)dE}{\int_{E_{min}}^{E_{max}} Ef(E)dE}. \tag{5}$$

If the flux F is in units of photons cm^{-2} s^{-1}, the parameter K is defined as

$$K = \frac{\int_{1\mathrm{keV}/(1+z)}^{10^4\mathrm{keV}/(1+z)} Ef(E)dE}{\int_{E_{min}}^{E_{max}} f(E)dE}, \tag{6}$$

where $f(E)$ is spectral model of GRB. Then we can obtain the bolometric luminosity L of each GRB. In Figure 1, the blue dots show the bolometric luminosity of GRBs, and the line is the observational limit of *Swift*. The limit is chosen as a minimum flux $F_{\min} = 2.0 \times 10^{-8}$ erg s^{-1}cm^{-2}, which is consistent with that of Li (2008). So the limit luminosity at redshift z is given as $L_{\mathrm{limit}} = 4\pi d_{\mathrm{L}}^2(z) F_{\min}$.

3. Lynden-Bell's c^- method and nonparametric test method

Lynden-Bell's c^- method is an efficient method to determinate the distribution of luminosity and redshift of objects with truncated data sample, including quasars (Lynden-Bell 1971; Efron & Petrosian 1992; Petrosian 1993; Maloney & Petrosian 1999), galaxies (Kirshner et al. 1978; Merighi et al. 1986; Peterson et al. 1986; Loh & Spillar 1986) and GRBs (Lloyd-Ronning et al. 2002; Yonetoku et al. 2004; Wu et al. 2012; Yonetoku et al. 2014). Lynden-Bell (1971) used this method to derive the luminosity function and density evolution from quasars with observational selection for the first time. This method can break the degeneracy between luminosity function and formation rate. It is better to extract the luminosity evolution from the form of the luminosity function. If the parameters L and z in the distribution of luminosity and redshift $\Psi(L, z)$ are independent, we can rewrite $\Psi(L, z)$ as $\Psi(L, z) = \psi(L)\phi(z)$ (Efron & Petrosian 1992), where $\psi(L)$, the fraction of GRB brighter than L, is the cumulative luminosity function, and $\phi(z)$ is the redshift cumulative distribution. Unfortunately, the luminosity and the redshift of GRBs are not independent (Yonetoku et al. 2004; Kocevski & Liang 2006; Wu et al. 2012), so we should write the $\Psi(L, z)$ as $\Psi(L, z) = \psi_z(L)\phi(z)$ instead of $\Psi(L, z) = \psi(L)\phi(z)$, where $\psi_z(L)$ is the luminosity function of GRB at redshift z. If we remove the effect of the luminosity evolution $g(z)$, i.e. a transformation $L_0 = L/g(z)$, the transformed luminosity L_0 are independent of redshift. As a result, we can obtain $\Psi(L_0, z) = \phi(z)\psi(L_0)$. Using the relation $L = L_0 g(z)$, we can write the $\Psi(L, z)$ as $\Psi(L, z) = \psi_z(L)\phi(z) = \psi(L_0)\phi(z)$. Then the luminosity function of GRB at redshift z is $\psi_z(L) = \psi(L/g(z))$.

To get the form of luminosity evolution $g(z)$, we introduce a nonparametric test method proposed by Efron & Petrosian (1992), which has been widely used in previous literature (Petrosian 1993; Maloney & Petrosian 1999; Lloyd-Ronning et al. 2002; Yonetoku et al. 2004; Wu et al. 2012; Yonetoku et al. 2014). For the ith data in the (L, z) data set, we can

define J_i as (Efron & Petrosian 1992)

$$J_i = \{j | L_j \geq L_i, z_j \leq z_i^{max}\}, \tag{7}$$

where L_i is the ith GBR luminosity and $z_i^{\rm max}$ is the maximum redshift at which a GRB with luminosity L_i can be observed. This region is shown in Figure 1 as black line rectangle. The number of GRBs contained in this region is n_i. The number $N_i = n_i - 1$, which means taking the ith GRB out, is the same as c^- in Lynden-Bell (1971). Similarly, J_i' is defined as

$$J_i' = \{j | L_j \geq L_i^{lim}, z_j < z_i\}, \tag{8}$$

where $L_i^{\rm lim}$ is the minimum observable luminosity at that redshift z_i. This region is shown as red rectangle in Figure 1. The number of events contained within this region is M_i.

We first consider the n_i GRBs in black rectangle in Figure 1. The number of events that have redshift z less than or equal to z_i is defined as R_i. If L and z are independent, R_i is uniformly distributed between 1 and n_i (Efron & Petrosian 1992). The test statistic τ is (Efron & Petrosian 1992)

$$\tau \equiv \sum_i \frac{(R_i - E_i)}{\sqrt{V_i}}, \tag{9}$$

where $E_i = \frac{1+n_i}{2}$, $V_i = \frac{n_i^2-1}{12}$ are the expected mean and the variance of R_i respectively. If the R_i is exactly uniformly distributed between 1 to n_i, the samples of $R_i \leq E_i$ and $R_i \geq E_i$ should be nearly equal, and the test statistic τ will nearly be 0. If we choose a from of $g(z)$ that makes test statistic $\tau = 0$, the effect of the luminosity evolution can be removed by transformation of $L_0 = L/g(z)$.

The functional form of $g(z) = (1+z)^k$ has been used in previous papers (Lloyd-Ronning et al. 2002; Yonetoku et al. 2004; Wu et al. 2012; Lloyd-Ronning et al. 2002; Kocevski & Liang 2006; Yonetoku et al. 2014). We also use this form in this paper. Then we test the independence between $L_0 = L/g(z)$ and z by changing the value of k until the test statistic τ is zero. Figure 2 shows the value of test statistic τ as a function of k. From this figure, we find the best fit is $k = 2.43^{+0.41}_{-0.38}$ at 1σ confidence level. So we take the luminosity evolution form $g(z)$ as $g(z) = (1+z)^{2.43}$. A hypothesis of no luminosity evolution $k = 0$, is rejected at about 4.7σ confidence level. This value is similar with Yonetoku et al. (2004), whose k-value is $k = 2.60^{+0.15}_{-0.20}$ and $k = 0$ is rejected with about 8.0σ significance from pseudo-redshift GRBs. Wu et al. (2012) also found that the value of k is $k = 2.30^{+0.56}_{-0.51}$.

After converting the observed luminosity to non-evolving luminosity $L_0 = L/(1+z)^{2.43}$, we can derive the local cumulative luminosity function $\psi(L_0)$ with nonparametric method from the following equation (Lynden-Bell 1971; Efron & Petrosian 1992),

$$\psi(L_{0i}) = \prod_{j<i}(1 + \frac{1}{N_j}), \tag{10}$$

where $j < i$ means that GRB has luminosity L_{0j} larger than L_{0i}. The cumulative number distribution $\phi(z)$ can be obtained from

$$\phi(z_i) = \prod_{j<i}(1 + \frac{1}{M_j}), \tag{11}$$

where $j < i$ means that GRB has redshift z_j less than z_i. The comoving differential form of $\phi(z)$, which represents the cosmic formation rate of GRBs $\rho(z)$, is more interesting. The formation rate of GRBs can be written as,

$$\rho(z) = \frac{d\phi(z)}{dz}(1+z)(\frac{dV(z)}{dz})^{-1}, \tag{12}$$

where $(1 + z)$ results from the cosmological time dilation and $dV(z)/dz$ is the differential comoving volume, which can be expressed as

$$\frac{dV(z)}{dz} = 4\pi(\frac{c}{H_0})^3(\int_0^z \frac{dz}{\sqrt{1-\Omega_{\rm m}+\Omega_{\rm m}(1+z)^3}})^2 \frac{1}{\sqrt{1-\Omega_{\rm m}+\Omega_{\rm m}(1+z)^3}}. \tag{13}$$

4. Luminosity function and formation rate of GRBs

In this section, we present results on the luminosity function and cosmic formation rate of GRBs.

4.1. Luminosity function

As discussed above, we get the form of luminosity evolution as $g(z) = (1+z)^{2.43}$ by using the nonparametric τ test method. The non-evolving luminosity L_0 is defined as $L_0 = L/g(z)$, which is shown in Figure 3. Using this new data set, the luminosity function $\psi(L_0)$ can be derived by using Lynden Bell's c^- method, which is shown in Figure 4. As shown in Figure 4, the luminosity function $\psi(L_0)$ can be fitted with a broken power law after removing the redshift evolution. The form of luminosity function $\psi(L_0)$ for dimmer and brighter bursts are fitted by

$$\psi(L_0) \propto \begin{cases} L_0^{-0.14\pm0.02} & L_0 < L_0^b, \\ L_0^{-0.70\pm0.03} & L_0 > L_0^b, \end{cases} \tag{14}$$

where $L_0^b = 1.43\times10^{51}$ erg s^{-1} is the break point. This result is consistent with previous work (Lloyd-Ronning et al. 2002; Yonetoku et al. 2004; Kocevski & Liang 2006; Wu et al. 2012). It is necessary to point out that this luminosity function is only the present distribution

at $z = 0$ since the luminosity evolution is removed. The luminosity function $\psi_z(L)$ at redshift z will be $\psi_z(L) = \psi(L/g(z)) = \psi(L/(1+z)^{2.43})$. So the break luminosity at z is $L_z^b = L_0^b(1+z)^{2.43}$.

4.2. Formation rate of GRBs

Figure 5 presents the cumulative GRB formation rate $\phi(z)$. According to equation (12), in order to get the cosmic formation rate of GRBs, we need the differential form of cumulative number distribution $d\phi(z)/dz$. Figure 6 shows $(1+z)d\phi(z)/dz$ as function of redshift z. From this figure, we find that $(1+z)d\phi(z)/dz$ increases quickly at $z < 1$, then keeps approximately constant for $1 < z < 4$, and decreases sharply at $z > 4$ with a power-law form. But we are more interested in the comoving density rate. From equation (12), we can calculate the GRBs formation rate $\rho(z)$, which is shown in Figure 7. In Figure 7, the blue stepwise line represents the comoving cosmic formation of GRBs as a function of redshift, and the error bar gives the 1σ confidence level. The best-fitting power laws for different segments are

$$\rho(z) \propto \begin{cases} (1+z)^{0.04\pm0.94} & z < 1, \\ (1+z)^{-0.94\pm0.11} & 1 < z < 4, \\ (1+z)^{-4.36\pm0.48} & z > 4, \end{cases} \tag{15}$$

with 95% confidence level. From this equation, we can derive the formation rate of GRBs at the local universe $\rho(0) = 7.3 \pm 2.7$ Gpc^{-3} yr^{-1}, which is larger than previous studies, e.g., $\rho(0) \sim 1.5$ Gpc^{-3} yr^{-1} (Schmidt 1999), $\rho(0) \sim 0.5$ Gpc^{-3} yr^{-1} (Guetta et al. 2005), and $\rho(0) > 0.5$ Gpc^{-3} yr^{-1} (Pélangeon et al. 2008). The main reason is that the GRB rate keeps constant at low redshift in this paper, while it increases fast in other studies. But Liang et al. (2007) found that the rate of low-luminosity GRBs is $\rho(0) \sim 325$ Gpc^{-3} yr^{-1}. This local rate is not corrected for the jet beaming effect.

Obviously, the formation rate of GRBs is in contrast to previous estimates of the comoving rate density by Yonetoku et al. (2004), Kocevski & Liang (2006) and Wu et al. (2012) with the same method. Our results shows that the formation rate of GRBs is almost constant at $z < 1.0$. But previous results give that the formation rate increases quickly at $z < 1.0$ (Yonetoku et al. 2004; Kocevski & Liang 2006; Wu et al. 2012), which is consistent with SFR observation (Hopkins & Beacon 2006). But our result is consistent with that of Petrosian et al. (2009) well. Interestingly, the evolution of $(1+z)d\phi(z)/dz$ shown in Figure 6, is consistent with the behavior of $\rho(z)$ in Wu et al. (2012). We also test our program with the same GRB data of Yonetoku et al. (2004) and Wu et al. (2012), and find that our $(1+z)d\phi(z)/dz$ shows the same behaviors as the $\rho(z)$ in Yonetoku et al. (2004)

and Wu et al. (2012). So they might omit the $dV(z)/dz$ term in their calculations. Besides, Yonetoku et al. (2004) and Wu et al. (2012) showed that the GRB rate increases as $(1+z)^{6.0\pm1.4}$ and $(1+z)^{8.24\pm4.48}$ at $z<1$ respectively, which are much quickly than $(1+z)^{2.4}$ of Kocevski & Liang (2006).

Several comprehensive works studying the luminosity function and the rate of long GRBs have been recently published using different methods (such as Wanderman & Piran 2010; Butler et al. 2010). Assuming that the luminosity function is redshift independent, Wanderman & Piran (2010) found that the power law index of luminosity function is 0.22 at low luminosity, and 1.4 at high luminosity with break $10^{52.5}$ erg s^{-1} using long GRBs with redshifts determined from afterglow. The formation rate increases as $(1+z)^{2.1}$ up to $z\sim3.0$ and it decreases as $(1+z)^{-1.4}$ at $z>3.0$. Butler et al. (2010) derived that the luminosity function is nearly flat $\propto L^{-0.2}$ below break $10^{52.7}$ erg s^{-1}, and declines $\propto L^{-3.0}$ using a large sample of GRBs detected by *Swift*. The GRB rate is similar as that of Wanderman & Piran (2010). These results are different from our results. One reason is the GRB sample. We use the latest GRB sample, which have redshift observed by *Swift* and spectral parameters given by *Fermi-GBM* and *Konus-wind*. The luminosity function evolution may be the most important reason. Wanderman & Piran (2010) assumed no redshift evolution of luminosity function. In the fitting of Butler et al. (2010), no luminosity evolution is required to produce the observed number of GRBs. But strong evolution of luminosity function is found in literatures. The evolution of luminosity can be parameterized as $(1+z)^{1.4}$ (Lloyd-Ronning et al. 2002). Yonetoku et al. (2004) and Wu et al. (2012) found that the evolution factor is $g(z)=(1+z)^{2.60}$ and $g(z)=(1+z)^{2.30}$ respectively. Tan et al. (2013) found that the luminosity function of GRB evolves with a redshift-dependent break luminosity $L_b=1.2\times10^{51}(1+z)^2$ erg s^{-1}, which is similar with our result. Virgili et al. (2011) found that a evolution factor $(1+z)^{1.0\pm0.2}$ of luminosity function can fit the BATSE and Swift data. These works suggest that take a evolution factor into consideration is necessary. Besides, our GRB sample including those GRBs dimmer than 10^{51} erg s^{-1} is another important reason. For example, Kistler et al. (2008) found that the density of GRB is much higher at $z<1$ if they included GRBs dimmer than 10^{51} erg s^{-1}. In this work, we use Lynden-Bell c^- method to correct the data truncated effect and consider the evolution of GRB luminosity function. So we don't need to omit these dim GRBs.

The relation between SFR and formation rate of GRBs is attractive. We also compare our result with the observed SFR from Hopkins & Beacon (2006) in Figure 8. Obviously, it is consistent with the observed SFR at $z>1.0$, but remarkably different at $z<1.0$. This trend means that the formation rate of GRBs $\rho(z)$ does not trace SFR at low redshift $z<1.0$. But at high redshift $z>4.0$, our result is consistent with the SFR derived from GRBs (Yüksel et al. 2008; Wang & Dai 2009; Kistler et al. 2009; Wang 2013). This result is dif-

ferent with others in previous literatures (Lloyd-Ronning et al. 2002; Yonetoku et al. 2004; Kocevski & Liang 2006; Wu et al. 2012), but it is consistent with that of Petrosian et al. (2009). There are also some previous works shown that the long GRBs may not unbiased tracers of SFR at low redshift. A strong dependence of the GRB rate on host-galaxy properties out to $z \sim 1.0$ is found by Perley et al. (2013). So use GRBs as direct tracers of the cosmic SFR is cautious at $z < 1.0$ (Perley et al. 2013). Vergani et al. (2014) found that the mass distribution of long GRB host galaxy is different with the expected from star-forming galaxies observed in deep survey, which suggests that long GRBs are not unbiased tracers of star formation activity at least at $z < 1.0$. They also found that long GRB rate can directly trace the SFR starting from $z \sim 4$ and above.

5. Testing with Monte Carlo simulation

In this section, we use Monte Carlo simulation to test our results. Firstly, we simulate a set of data (L_0, z) which follows the distribution described by equation (14) and equation (15) using Monte Carlo method. Then, we transfer the luminosity L_0 to L through $L = L_0(1+z)^k$, where $k = 2.43$. So we can get sets of pseudo data of GRB luminosity and redshift (L, z). In the simulations, we create 200 pseudo samples. Each sample contains 130 GRBs. Then we use Lynden-Bell c^- method and nonparametric τ test method to calculate the distributions of these pseudo samples. Finally, we compare the simulated data with observed data.

Figure 9 shows the comparing results. The four panels give the luminosity-redshift distribution, luminosity function, cumulative distribution and $\log N - \log S$ distribution. In the panel a, we randomly choose one pseudo sample of GRB from the 200 samples to compare with the observed data. The red dots and the blue dots represent the observed data and the simulated data, respectively. From this panel, we can see that the simulated data and the observed data have similar distributions. The other three panels b, c and d show the comparisons of the luminosity function, cumulative distribution and $\log N - \log S$ distribution between the observed data and mock data. The red curves show the distributions of the observed data, blue curves give the distributions of all of the 200 pseudo samples of GRB data and the blue curves are the mean distributions of the 200 pseudo samples. We perform the Kolmogorov-Smirnov test between observed data and the mean distributions of simulated data. The chance probabilities of the three tests are 0.49, 0.86 and 0.96, respectively. From these panels, we can also conclude that the distribution of the observed data lie in the region of those pseudo data, which means that the derived luminosity function and formation rate of GRBs are correct.

In order to test whether long GRBs are unbiased tracers of SFR at low redshift, we

simulate 200 new pseudo samples of GRBs by assuming that the GRB rate follows the SFR from Yüksel et al. (2008), i.e., $\rho(z) \propto (1+z)^{3.4}$ at $z < 1$, $\rho(z) \propto (1+z)^{-0.3}$ at $1 < z < 4$ and $\rho(z) \propto (1+z)^{-3.5}$ at $z > 4$. Then we use the same method to calculate the distributions of these pseudo data. We find that the cumulative redshift distribution of observed data is not consistent with the pseudo data, which is shown in Figure 10. The red, blue and green curves have the same meanings as those in Figure 9. From Figure 10, we can see that part of the cumulative redshift distribution line of observed data lies outside of the region occupied by pseudo GRB data, especially at $z < 1.0$. The Kolmogorov-Smirnov test between the distribution from observed data and the mean distribution of simulated data gives the chance probability of $p = 6.9 \times 10^{-12}$. It means that long GRBs are not direct tracers of SFR at $z < 1.0$.

6. Conclusions and Discussions

In this paper, we use Lynden-Bell's c^- method to study the luminosity function and formation rate of *Swift* long GRBs without any assumptions. First, we use a τ statistical method to separate the luminosity evolution from the stable form of the luminosity function by choosing the evolution form $g(z) = (1+z)^k$. The most proper k is $k = 2.43^{+0.41}_{-0.38}$, which gives $\tau = 0$. This value is similar with those of Yonetoku et al. (2004), Wu et al. (2012) and Kocevski & Liang (2006). After correcting the luminosity evolution by $L_0 = L/(1+z)^{2.43}$, the cumulative luminosity function $\psi(L_0)$ and cumulative number distribution $\phi(z)$ of GRBs can be calculated, which are shown in Figure 4 and Figure 5. The luminosity function of GRBs can be well fitted with a broken power law form as $\psi(L_0) \propto L_0^{-0.14\pm0.02}$ and $\psi(L_0) \propto L_0^{-0.70\pm0.03}$ for $L_0 < L_0^{\rm b}$ and $L_0 > L_0^{\rm b}$ respectively, where $L_0^{\rm b} = 1.43 \times 10^{51}$ erg s^{-1} is the break point.

We also derive the formation rate of GRBs through the differential form of the cumulative number distribution $\phi(z)$. Figure 6 shows the evolution of $(1+z)\frac{d\phi(z)}{dz}$. We find that $(1+z)\frac{d\phi(z)}{dz}$ increases quickly at $z < 1$, then remains roughly constant at $1 < z < 4$ and finally decreases rapidly at high redshift. From equation (12), the cosmic formation rate of GRBs $\rho(z)$ is derived, which is shown in Figure 7. The best-fitting power laws for different redshift segments are $\rho(z) \propto (1+z)^{0.04}$, $\rho(z) \propto (1+z)^{-0.94}$, $\rho(z) \propto (1+z)^{-4.36}$ for $z < 1.0$, $1.0 < z < 4.0$ and $z > 4.0$ respectively. Our results show that the formation rate of GRBs is almost constant at $z < 1.0$. But previous results give that the formation rate increases quickly at $z < 1.0$ (Yonetoku et al. 2004; Kocevski & Liang 2006; Wu et al. 2012). But Yonetoku et al. (2004) and Kocevski & Liang (2006) used the pseudo redsihfts of GRBs rather than the observed redshifts. Besides, we find the $\rho(z)$ in Wu et al. (2012) and

Yonetoku et al. (2004) increase fast at $z < 1.0$, which has the similar behavior of $(1+z)\frac{d\phi(z)}{dz}$ shown in Figure 6. So they might omit the $dV(z)/dz$ term in their calculations. From Figure 8, it is easily to find that GRB formation rate $\rho(z)$ is consistent with observed SFR at $z > 1.0$ but entirely different at $z < 1.0$. It means that the formation rate of GRBs only traces SFR at $z > 1.0$, which is different with previous work (Yonetoku et al. 2004; Kocevski & Liang 2006; Wu et al. 2012). We find the low-redshift excess of GRB rate for the first time.

Surprisingly, we find that formation rate of GRBs is consistent with SFR at $z > 1.0$, but shows an excess at low redshift $z < 1.0$ for the first time, which is different with previous works. Our result shows that formation rate of GRBs is larger than SFR at $z < 1.0$. Below, we will discuss some possible reasons for this low-redshift excess.

The first one is that the definition of long GRBs is not clear. In classical method, the long GRBs are defined by $T_{90} > 2$ s (Kouveliotou et al. 1993). There is no clear boundary line in this diagram to separate the long and short GRBs. Moreover, T_{90} is an observed time scale, which represents different time for GRBs at different redshifts. Meanwhile, the observations of low-redshift long GRBs, such as GRB 060614 at $z = 0.125$ and GRB 060505 at $z = 0.089$, show no association of supernovae (Gal-Yam et al. 2006; Fynbo et al. 2006; Gehrels et al. 2006). So more physical criterions are required to classify GRBs. Because only a subclass of GRBs can trace the SFR. Some attempts have been performed (Zhang 2006; Zhang et al. 2007, 2009; Bloom et al. 2008; Bromberg et al. 2013; Lü et al. 2014). It has been suggested that GRBs can be classified physically into Type I (compact star origin) and Type II (massive star origin) (Zhang 2006; Zhang et al. 2007).

The second one is that some selection effects have not been included in analysis. For example, it is easier to measure the redshift of those GRBs which are in lower redshift and therefore create a bias toward low redshift GRBs. It means that we lose some high redshift GRBs, so the formation rate of GRBs at low redshift we calculated will larger than the SFR. This bias can be removed by using samples with high completeness in the GRB redshift measurements. There are three of such a sample in previous literature (Greiner et al. 2011; Salvaterra et al. 2012; Hjorth et al. 2012). It could be considered in the future works.

The third one is that there may exist a subclass GRBs, i.e., low-luminosity GRBs (Cobb et al. 2006; Pian et al. 2006; Soderberg et al. 2006; Liang et al. 2007). The local rate of low-luminosity GRBs may be high, i.e., $\rho(0) = 100-1000\,\mathrm{yr}^{-1}\,\mathrm{Gpc}^{-3}$(Soderberg et al. 2006; Liang et al. 2007), much higher than high-luminosity GRBs. The progenitors of low-luminosity GRBs may be different with those of high-luminosity GRBs (Mazzali et al. 2006; Soderberg et al. 2006). The contamination from low-luminosity GRBs could lead to the low-redshift excess.

We thank the referee for helpful commentary on the manuscript. We acknowledge the use of public data from the *Swift* data archive. We thank Bing Zhang, Yun-Wei Yu, Shi-Wei Wu and Jin-Jun Geng for helpful discussions. This work is supported by the National Basic Research Program of China (973 Program, grant No. 2014CB845800), the National Natural Science Foundation of China (grants 11422325, 11373022, 11033002, and J1210039), the Excellent Youth Foundation of Jiangsu Province (BK20140016), and the Program for New Century Excellent Talents in University (grant No. NCET-13-0279). KSC is supported by the CRF Grants of the Government of the Hong Kong SAR under HUKST4/CRF/13G.

REFERENCES

Band, D., Matteson, J., Ford, L., et al., 1993, ApJ, 413, 281

Barbier, L., Barthelmy, S., Cummings, J., et al., 2006, GCN, 4518

Barbier, L., Barthelmy, S., Cummings, J., et al., 2007, GCN, 6623

Barger, A. J., Cowie, L. L., & Richards, E. A., 2000, AJ, 119, 2092

Barthelmy, S. D., Baumgartner, W. H., Cummings, J. R., et al., 2009, GCN, 10103

Barthelmy, S. D., Baumgartner, W. H., Cummings, J. R., 2013, GCN, 10103

Bloom, J. S., Butler, N. R., & Perley, D. A. 2008, in AIP Conf. Ser. 1000, Gamma-Ray Bursts 2007: Proceedings of the Santa Fe Conf., ed.M. Galassi, D. Palmer, & E. Fenimore (Melville, NY: AIP), 11

Bloom, J. S., Frail, D. A., & Sari, R., 2001, AJ, 112, 2879

Bouwens, R. J., Illingworth, G. D., Labbe, I., et al. 2011, Nature, 479, 504

Briggs, M. S. & Younes, G., 2011, GCN, 12744

Bromberg, O., Nakar, E., Piran, T., & Sari, R., 2013, ApJ, 764, 179

Broom, V., & Loeb, A., 2002, ApJ, 575, 111

Bromm, V., Loeb, A., 2012, in Gamma-ray Bursts, ed. C. Kouveliotou, S. E. Woosley, R. A. M. J. Wijers (Cambridge: Cambridge Univ. Press), arXiv:0706.2445v2

Butler, N. R., Kocevski, D., Bloom, J. S., & Curtis, J. L., 2007, ApJ, 671, 656

Butler, N. R., Bloom, J. S. & Poznanski, D. 2010, ApJ, 711, 495

Cao, X. F., Yu, Y. W., Cheng, K. S., & Zheng, X. P., 2011, MNRAS, 416, 2174

Castro-Tirado, A. J., Sánchez-Ramírez, R., Ellison, S. L., et al., 2013, arXiv:1312.5631

Chaplin, V., 2012, GCN, 13737

Cheng, K. S., Yu, Y., & Harko, T., 2010, Phys. Rev. Lett., 104, 241102

Cobb, B. E., Bailyn, C. D., van Dokkum, P. G., & Natarajan, P. 2006, ApJ, 645, L113

Collazzi, A. C., 2012, GCN, 13145

Coward, D., 2007, New Astronomy Reviews, 51, 539

Dai, Z. G., Liang, E. W., & Xu, D., 2004, ApJ, 612, L101

Efron, B. & Petrosian, V. 1992, ApJ, 399, 345

Elliott, J., Greiner, J., Khochfar, S., et al. 2012, A&A, 539, A113

Elliott, J., Khochfar, S., Greiner, J., Dalla Vecchia, C., 2014, arXiv:1408.2526

Fenimore, E. E. & Ramirez-Ruiz, E. 2000, arXiv:astro-ph/0004176

Firmani, C., Avila-Reese, V., Ghisellini, G., & Tutukov, A. V. 2004, ApJ, 611, 1033

Fitzpatrick, G., 2010a, GCN, 11124

Fitzpatrick, G., 2010b, GCN, 11128

Fitzpatrick, G. & Pelassa, V., 2013, GCN, 14858

Fitzpatrick, G., 2013, GCN, 14896

Foley, S. & Briggs, M., 2010, GCN, 10851

Foley, S., 2011, GCN, 10851

Fynbo, J. P. U., Watson, D., Thone, C. C., et al., 2006, Natur, 444, 1047

Gal-Yam, A., Fox, D. B., Price, P. A., et al., 2006, Natur, 444, 1053

Gehrels, N., Norris, J. P., Barthelmy, S. D., et al., 2006, Natur, 444, 1044

Gehrels, N., Ramirez-Ruiz, E., & Fox, D. B., 2009, ARA&A, 47, 567

Golenetskii, S., Aptekar, R., Mazets, E., et al., 2005a, GCN, 3179

Golenetskii, S., Aptekar, R., Mazets, E., et al., 2005b, GCN, 3518

Golenetskii, S., Aptekar, R., Mazets, E., et al., 2005c, GCN, 4238

Golenetskii, S., Aptekar, R., Mazets, E., et al., 2006a, GCN, 4599

Golenetskii, S., Aptekar, R., Mazets, E., et al., 2006b, GCN, 5264

Golenetskii, S., Aptekar, R., Mazets, E., et al., 2006c, GCN, 5459

Golenetskii, S., Aptekar, R., Mazets, E., et al., 2006d, GCN, 5722

Golenetskii, S., Aptekar, R., Mazets, E., et al., 2006e, GCN, 5748

Golenetskii, S., Aptekar, R., Mazets, E., et al., 2006f, GCN, 5837

Golenetskii, S., Aptekar, R., Mazets, E., et al., 2007a, GCN, 6403

Golenetskii, S., Aptekar, R., Mazets, E., et al., 2007b, GCN, 6849

Golenetskii, S., Aptekar, R., Mazets, E., et al., 2007c, GCN, 6879

Golenetskii, S., Aptekar, R., Mazets, E., et al., 2007d, GCN, 6960

Golenetskii, S., Aptekar, R., Mazets, E., et al., 2007e, GCN, 7114

Golenetskii, S., Aptekar, R., Mazets, E., et al., 2007f, GCN, 7155

Golenetskii, S., Aptekar, R., Mazets, E., et al., 2008a, GCN, 7487

Golenetskii, S., Aptekar, R., Mazets, E., et al., 2008b, GCN, 7589

Golenetskii, S., Aptekar, R., Mazets, E., et al., 2008c, GCN, 7812

Golenetskii, S., Aptekar, R., Mazets, E., et al., 2008d, GCN, 7854

Golenetskii, S., Aptekar, R., Mazets, E., et al., 2008d, GCN, 7862

Golenetskii, S., Aptekar, R., Mazets, E., et al., 2009, GCN, 10083

Golenetskii, S., Aptekar, R., Frederiks, D., et al., 2010a, GCN, 11021

Golenetskii, S., Aptekar, R., Frederiks, D., et al., 2010b, GCN, 11119

Golenetskii, S., Aptekar, R., Frederiks, D., et al., 2010c, GCN, 11251

Golenetskii, S., Aptekar, R., Mazets, E., et al., 2011a, GCN, 11971

Golenetskii, S., Aptekar, R., Frederiks, D., et al., 2011b, GCN, 12166

Golenetskii, S., Aptekar, R., Mazets, E., et al., 2011c, GCN, 12223

Golenetskii, S., Aptekar, R., Frederiks, D., et al., 2011d, GCN, 12270

Golenetskii, S., Aptekar, R., Frederiks, D., et al., 2011e, GCN, 12433

Golenetskii, S., Aptekar, R., Frederiks, D., et al., 2013a, GCN, 14368

Golenetskii, S., Aptekar, R., Frederiks, D., et al., 2013b, GCN, 14575

Golenetskii, S., Aptekar, R., Frederiks, D., et al., 2013c, GCN, 14958

Golenetskii, S., Aptekar, R., Frederiks, D., et al., 2013d, GCN, 15145

Golenetskii, S., Aptekar, R., Frederiks, D., et al., 2013e, GCN, 15203

Golenetskii, S., Aptekar, R., Frederiks, D., et al., 2013f, GCN, 15413

Greiner, J., Krühler, T., Fynbo, J. P. U., et al., 2009, ApJ, 693, 1610

Greiner, J., Krühler, T., Klose, S., 2011, A&A, 526, 30

Gruber, D., 2010, GCN, 11454

Gruber, D., 2012a, GCN, 12874

Gruber, D., 2012b, GCN, 13469

Guetta, D., & Piran, T., 2007, J. Cosmol. Astropart. Phys., 7, 3

Guetta, D., Piran, T., & Waxman, E., 2005, ApJ, 619, 412

Hjorth, J., et al., 2003, Nature, 423, 847

Hjorth, J., Malesani, D., Jakobsson, P., et al., 2012, ApJ, 756, 187

Hopkins, A. M., & Beacon, J. F. 2006, ApJ, 651, 142

Howell, E. J., Coward, D. M., Stratta, G., Gendre, B., & Zhou, H., arXiv: 1407.2333

Kirshner, R. P., Oemler, A. & Schechter, P. L., 1978, AJ, 83, 1549

Kistler, M. D., Yüksel, H., Beacom, J. F. & Stanek, K. Z., 2008, ApJ, 673, L119

Kistler, M. D., Yüksel, H., Beacom, J. F., Hopkins, A. M. & Wyithe, J. S. B., 2009, ApJ, 705, L104

Kocevski, D., & Liang, E., 2006, ApJ, 642, 371

Kouveliotou, C., Meegan, C., A., Fishman, G. J., et al., 1993, ApJ, 413, L101

Lamb, D. Q., & Reichart, D. E. 2000, ApJ, 536, 1

Le, T., & Dermer, C. D. 2007, ApJ, 661, 394

Li, L. X. 2008, MNRAS, 388, 1487

Liang, E. W., Zhang, B., Virgili, F., & Dai, Z. G., 2007, ApJ, 662, 1111

Lilly, S. J., Lefevre, O., Hammer, F., & Crampton, D. 1996, ApJ, 460, L1

Lin, J. R., Zhang, S. N., & Li, T. P., 2004, ApJ, 605, 819

Llyd-Ronning, N. M., Fryer, C. L. & Ramirez-Ruiz, E., 2002, ApJ, 574, 554

Loh, E. D. & Spillar, E. J., 1986, ApJ, 307, L1

Lü, H., Zhang, B., Liang, E. W., Zhang, B. B., & Sakamoto, T., 2014, MNRAS, 442, 1922

Lynden-Bell, D., 1971, MNRAS, 155, 95

Maloney, A., & Petrosian, V. 1999, ApJ, 518, 32

Mazzali, P. A., Deng, J., Nomoto, K., et al. 2006, Nature, 442, 1018

McBreen, S., 2009, GCN, 9415

McGlynn, S., 2012, GCN, 14012

McQuinn, M., Lidz, A., Zaldarriaga, M., Hernquist, L. & Dutta, S., 2008, MNRAS, 388, 1101

Merighi, R., Marano, B. & Vettolani, G., 1986, A&A, 160, 398

Mészáros, P., 2006, Rep. Prog. Phys., 69, 2259

Nava, L., Ghirlanda, G., Ghisellini G., et al., 2011, A&A, 530, A21

Nava, L., Salvaterra, R., Ghirlanda, G., et al., 2012, MNRAS, 421, 1256

Ohno, M., Uehara, T., Takahashi, T., et al., 2007, GCN, 6638

Ohno, M., Kokubun, M., Suzuki, M., et al., 2008, GCN, 7630

Pal'Shin, V., Golenetskii, S., Aptekar, R., Mazets, E., et al., 2008, GCN, 8256

Pal'Shin, V., Golenetskii, S., Aptekar, R., Mazets, E., et al., 2013, GCN, 14702

Pélangeon, A., et al., 2008, A&A, 491, 157.

Pelassa, V., 2011, GCN, 12545

Perley, D. A., Levan, A. J., Tanvir, N. R., et al., 2013, ApJ, 778, 128

Peterson, B. A., Ellis, R. S., Efstathiou, G., Shanks, T., Bean, A. J., Fong, R. & Zen-Long, Z., 1986, MNRAS, 221, 233

Petrosian, V. 1993, ApJ, 402, L33

Petrosian, V., Bouvier, A. & Ryde, F., 2009, arXiv:0909.5051v1

Pian, E., Mazzali, P. A., Masetti, N., et al. 2006, Nature, 442, 1011

Porciani, C., & Madau, P. 2001, ApJ, 548, 522

Qin, S. F., Liang, E. W., Lu, R. J., Wei, J. Y., & Zhang, S. N. 2010, MNRAS, 406, 558

Sakamoto, T., Barbier, L., Barthelmy, S., et al., 2006, GCN, 5029

Sakamoto, T., Barthelmy, S. D., Baumgartner, W., et al., 2008, GCN, 8101

Sakamoto, T., Barthelmy, S. D., Baumgartner, W., et al., 2011, GCN, 12276

Salvaterra, R., & Chincarini, G., 2007a, ApJ, 656, L49

Salvaterra, R., Della Valle, M., Campana, S., et al., 2009, Nature, 461, 1258

Salvaterra, R., Guidorzi, C., Campana, S., Chincarini, G., & Tagliaferri, G., 2009, MNRAS, 396, 299

Salvaterra, R., Campana, S., Vergani, S. D., et al., 2012, ApJ, 749, 68

Schaefer B. E., 2007, ApJ, 660, 16

Schmidt, M., 1999, ApJ, 523, L117

Soderberg, A. M., Kulkarni, S. R., Nakar, E., et al. 2006, Nature, 442, 1014

Stamatikos, M., Barbier, L., Barthelmy, S., et al., 2006, GCN, 5289

Stamatikos, M., Barthelmy, S. D., Cummings, J., et al., 2008, GCN, 7277

Stanek, K. Z., Matheson, T., Garnavich, P. M., et al., 2003, ApJ, 591, L17

Sugita, S., Yamaoka, K., Ohno, M., et al., 2009, PASJ, 61, 521

Tan, W. W., Cao, X. F., & Yu, Y. W., 2013, ApJL, 772, L8

Tanvir, N. R., Fox, D. B., LevanA, J., et al., 2009, Nature, 461, 1254

Totani, T., 1997, ApJ, 486, L71

Totani, T., Kawai, N., Kosugi, G., et al. 2006, PASJ, 58, 485

Tueller, J., Barthelmy, S. D., Baumgartner, W., et al., 2008, GCN, 7604

van der Horst, A. J., 2010, GCN, 11477

Vergani, S. D., Salvaterra, R., Japelj, J., et al., 2014, arXive:1409.7064

von Kienlin, A., 2013, GCN, 14473

Virgili, F. J., Zhang, B., Nagamine, K., & Choi, J. H. 2011, MNRAS, 417, 3025

Wanderman, D. & Piran, T. 2010, MNRAS, 406, 1944

Wang, F. Y., Bromm, V., Greif. T. H., Stacy, A., Dai, Z. G., Loeb, A. & Cheng, K. S., 2012, ApJ, 760, 27

Wang, F. Y., & Dai, Z. G. 2009, MNRAS, 400, L10

Wang, F. Y., & Dai, Z. G. 2011a, ApJL, 727, 34

Wang, F. Y., & Dai, Z. G. 2014, ApJS, 213, 15

Wang, F. Y., Dai, Z. G., & Liang, E. W., 2015, arXiv: 1504.00735

Wang, F. Y., Qi, S. & Dai, Z. G. 2011, MNRAS, 415, 3423

Wang, F. Y., 2013, A&A, 556, A90

Wijers, R. A. M., Bloom, J. S., Bagla, J. S. & Natarajan, P., 1998, MNRAS, 294, L13

Woosley, S. E. 1993, ApJ, 405, 273

Wu, S. W., Xu, D., Zhang, F. W. & Wei, D. M., 2012, MNRAS, 423, 2627

Xiong, S., 2011, GCN, 12287

Xiong, S. & Rau, A., 2013, GCN, 14429

Yonetoku, D., Murakami, T., Nakamura, T., Yamazaki, R., Inoue, A. K. & Ioka, K., 2004, ApJ, 609, 935

Yonetoku, D., Nakamura, T., Sawano, T., Takahashi, K., Toyanago, A., 2014, ApJ, 789, 65

Younes, G. & Barthelmy, S. D., 2012, GCN, 13722

Younes, G., 2012, GCN, 13809

Younes, G. & Bhat, P. N., 2013, GCN, 14219

Yu, D., 2012, GCN, 14078

Yüksel, H., Kistler, M. D., Beacom, J. F. & Hopkins, A. M., 2008, ApJ, 683, L5

Zhang, B., 2006, Nature, 444, 1010

Zhang, B., 2007, Chin. J. Astron. Astrophys., 7, 1

Zhang, B., Liang, E. W., Page, K. L., et al. 2007, ApJ, 655, 989

Zhang, B., Zhang, B. B., Virgili, F. J., et al., 2009, ApJ, 703, 1696

Table 1. List of long GRBs used in this paper. It gives the name, redshift z, spectra parameters α & β, rest frame peak energy E_p, peak flux F, energy range, bolometric luminosity L in $1 - 10^4$ keV and reference of the parameters of spectrum of each GRB.

GRB	z	α	β^b	E_p(keV)	Flux(erg/cm^2/s)	Range(keV)	L(erg/s)	Ref.
050318	1.44	$-1.34^{+0.32}_{-0.32}$	...	$63.52^{+11.07}_{-11.07}$	$(2.2 \pm 0.17) \times 10^{-7}$	15 - 150	$4.96^{+0.38}_{-0.38} \times 10^{51}$	1
050401	2.9	$-0.83^{+0.21}_{-0.21}$	$-2.37^{+0.14}_{-0.14}$	119^{+26}_{-26}	$(2.45 \pm 0.12) \times 10^{-6}$	20 - 2000	$2.09^{+0.10}_{-0.10} \times 10^{53}$	2
050416A	0.6535	-1.0	-3.4	$15.73^{+2.42}_{-2.42}$	5 ± 0.5^a	15 - 150	$9.89^{+0.99}_{-0.99} \times 10^{50}$	1
050525	0.606	$-0.99^{+0.11}_{-0.11}$	...	$79.08^{+3.74}_{-3.74}$	47.7 ± 1.2^a	15 - 150	$9.00^{+0.23}_{-0.23} \times 10^{51}$	1
050603	2.821	$-0.79^{+0.06}_{-0.06}$	$-2.15^{+0.09}_{-0.09}$	349^{+28}_{-28}	$(3.2 \pm 0.2) \times 10^{-5}$	20 - 3000	$2.25^{+0.14}_{-0.14} \times 10^{54}$	3
050802	1.71	$-1.6^{+0.1}_{-0.1}$	...	> 70.59	$(2.21 \pm 3.53) \times 10^{-7}$	15 - 150	$> 9.34 \times 10^{51}$	1
050904	6.29	$-1.15^{+0.12}_{-0.12}$	...	314^{+173}_{-89}	$(1.84 \pm 0.41) \times 10^{-7}$	15 - 5000	$9.25^{+2.06}_{-2.06} \times 10^{52}$	4
050922C	2.198	$-0.83^{+0.24}_{-0.24}$	...	$130.8^{+36.9}_{-36.9}$	$4.5^{+0.72}_{-1.53} \times 10^{-6}$	20 - 2000	$1.95^{+0.30}_{-0.30} \times 10^{53}$	1
051001	2.4296	$-1.12^{+0.66}_{-0.56}$	...	$44.38^{+11.48}_{-11.48}$	$1.95^{+0.83}_{-0.57} \times 10^{-8}$	15 - 350	$1.38^{+0.59}_{-0.40} \times 10^{51}$	5
051109A	2.346	$-1.25^{+0.44}_{-0.59}$	...	161^{+224}_{-58}	$5.8^{+0.3}_{-4.9} \times 10^{-7}$	20 - 500	$3.40^{+0.18}_{-2.87} \times 10^{52}$	6
051111	1.55	$-0.98^{+0.25}_{-0.24}$	...	$179.70^{+316.76}_{-54.52}$	$3.41^{+0.66}_{-0.52} \times 10^{-7}$	15 - 350	$7.04^{+1.36}_{-1.07} \times 10^{51}$	5
060115	3.53	$-1.0^{+0.5}_{-0.5}$	...	62^{+31}_{-10}	0.9 ± 0.1^a	15 - 150	$1.04^{+0.12}_{-0.12} \times 10^{52}$	7
060124	2.296	$-1.29^{+0.14}_{-0.11}$	$-2.25^{+0.27}_{-0.88}$	$247.76^{+130.91}_{-88.75}$	$2.66^{+0.74}_{-0.69} \times 10^{-6}$	20 - 2000	$1.37^{+0.38}_{-0.35} \times 10^{53}$	8
060206	4.048	$-1.12^{+0.3}_{-0.3}$	...	81^{+22}_{-22}	$(2.02 \pm 0.13) \times 10^{-7}$	15 - 150	$5.29^{+0.34}_{-0.34} \times 10^{52}$	1
060210	3.91	$-1.12^{+0.26}_{-0.26}$	...	117^{+23}_{-23}	2.8 ± 0.3^a	15 - 150	$5.64^{+0.60}_{-0.60} \times 10^{52}$	1
060306	3.5	$-1.2^{+0.5}_{-0.5}$	...	70^{+18}_{-18}	$(4.71 \pm 0.278) \times 10^{-7}$	15 - 150	$8.85^{+0.51}_{-0.51} \times 10^{52}$	1
060428B	0.348	$-0.94^{+1.30}_{-1.30}$	...	21.7^{+14}_{-14}	0.6 ± 0.1^a	15 - 150	$2.15^{+0.36}_{-0.36} \times 10^{49}$	9
060614	0.125	$-1.57^{+0.12}_{-0.14}$	...	302^{+214}_{-85}	$(4.5 \pm 0.7) \times 10^{-6}$	20 - 2000	$2.33^{+0.37}_{-0.79} \times 10^{50}$	10
060707	3.425	$-0.66^{+0.63}_{-0.63}$	...	66^{+25}_{-10}	1.1 ± 0.2^a	15 - 150	$1.12^{+0.20}_{-0.20} \times 10^{52}$	11
060708	1.92	$-0.93^{+0.47}_{-0.43}$	...	$87.45^{+83.35}_{-18.94}$	$1.78^{+0.45}_{-0.33} \times 10^{-7}$	15 - 350	$5.82^{+1.47}_{-1.08} \times 10^{51}$	5
060814	0.84	$-1.43^{+0.16}_{-0.16}$	...	257^{+122}_{-58}	$(2.13 \pm 0.35) \times 10^{-6}$	20 - 1000	$9.46^{+1.55}_{-1.55} \times 10^{51}$	12
060908	1.8836	$-0.93^{+0.25}_{-0.25}$	...	148^{+72}_{-72}	$(2.81 \pm 0.23) \times 10^{-7}$	15 - 150	$1.34^{+0.11}_{-0.11} \times 10^{52}$	1
060927	5.47	$-0.81^{+0.36}_{-0.36}$	...	71^{+14}_{-14}	$(2.47 \pm 0.17) \times 10^{-7}$	15 - 150	$1.16^{+0.08}_{-0.08} \times 10^{53}$	1
061007	1.261	$-0.53^{+0.09}_{-0.08}$	$-2.61^{+0.25}_{-0.49}$	498^{+54}_{-48}	$1.95^{+0.31}_{-0.24} \times 10^{-5}$	20 - 10000	$1.78^{+0.28}_{-0.22} \times 10^{53}$	13
061021	0.3463	$-1.22^{+0.12}_{-0.14}$	...	777^{+549}_{-237}	$3.72^{+0.53}_{-1.62} \times 10^{-6}$	20 - 2000	$1.76^{+0.25}_{-0.77} \times 10^{51}$	14
061121	1.314	$-1.32^{+0.04}_{-0.05}$	...	606^{+90}_{-72}	$1.28^{+0.16}_{-0.19} \times 10^{-5}$	20 - 5000	$1.48^{+0.19}_{-0.22} \times 10^{53}$	15
061222A	2.088	$-1.00^{+0.05}_{-0.05}$	$-2.32^{+0.38}_{-0.38}$	353^{+54}_{-54}	$(4.8 \pm 1.3) \times 10^{-6}$	20 - 10000	$1.48^{+0.40}_{-0.40} \times 10^{53}$	1
070110	2.352	$-1.15^{+0.45}_{-0.41}$	...	$108.33^{+183.02}_{-16.29}$	$(5.168 \pm 0.831) \times 10^{-6}$	15 - 350	$2.95^{+0.87}_{-0.59} \times 10^{51}$	5
070129	2.3384	$-1.33^{+0.68}_{-0.59}$	...	$65.96^{+179.79}_{-63.48}$	$2.72^{+0.8}_{-0.55} \times 10^{-8}$	15 - 350	$1.72^{+0.51}_{-0.35} \times 10^{51}$	5
070306	1.497	$-1.67^{+0.1}_{-0.1}$	...	> 105	$(3.04 \pm 0.164) \times 10^{-7}$	15 - 150	$> 1.04 \times 10^{52}$	1
070508	0.82	$-0.81^{+0.07}_{-0.07}$	...	188^{+8}_{-8}	$8.3^{+1.03}_{-1.11} \times 10^{-6}$	20 - 1000	$2.96^{+0.37}_{-0.40} \times 10^{52}$	16
070714B	0.92	$-0.86^{+0.1}_{-0.1}$	...	1120^{+780}_{-380}	2.7 ± 0.2^a	15 - 150	$1.22^{+0.09}_{-0.09} \times 10^{52}$	17,18
070810A	2.17	$-0.75^{+0.83}_{-0.69}$	...	$42.23^{+6.62}_{-6.46}$	$9.92^{+4.1}_{-2.88} \times 10^{-8}$	15 - 350	$4.92^{+2.04}_{-1.43} \times 10^{51}$	19
071003	1.605	$-0.76^{+0.06}_{-0.07}$	...	780^{+81}_{-70}	$1.22^{+0.19}_{-0.22} \times 10^{-5}$	20 - 4000	$2.18^{+0.34}_{-0.39} \times 10^{53}$	20
071010B	0.947	$-1.25^{+0.74}_{-0.49}$	$-2.65^{+0.29}_{-0.49}$	52^{+10}_{-14}	$8.92^{+2.99}_{-5.99} \times 10^{-7}$	20 - 1000	$6.47^{+2.17}_{-4.34} \times 10^{51}$	21
071020	2.145	$-0.65^{+0.27}_{-0.32}$	...	322^{+80}_{-53}	$6.04^{+1.22}_{-3.88} \times 10^{-6}$	20 - 2000	$2.25^{+0.45}_{-1.44} \times 10^{53}$	22
071117	1.331	$-1.53^{+0.15}_{-0.16}$	...	278^{+236}_{-79}	$6.66^{+1.13}_{-2.95} \times 10^{-6}$	20 - 1000	$9.95^{+1.69}_{-4.41} \times 10^{52}$	23
071227	0.383	-0.7	...	1000	$(3.5 \pm 1.1) \times 10^{-6}$	20 - 1300	$2.52^{+0.79}_{-0.79} \times 10^{51}$	24
080207	2.0858	$-1.17^{+0.27}_{-0.27}$	...	$107.8^{+72.5}_{-72.5}$	1.0 ± 0.3^a	15 - 150	$4.22^{+1.27}_{-1.27} \times 10^{51}$	25
080319B	0.937	$-0.86^{+0.01}_{-0.01}$	$-3.59^{+0.45}_{-0.45}$	675^{+22}_{-22}	$(2.26 \pm 0.21) \times 10^{-5}$	20 - 7000	$1.05^{+0.10}_{-0.10} \times 10^{53}$	1
080319C	1.95	$-1.01^{+0.13}_{-0.13}$	$-1.87^{+0.15}_{-0.63}$	307^{+141}_{-92}	$3.35^{+0.79}_{-0.7} \times 10^{-6}$	20 - 4000	$9.46^{+2.23}_{-1.98} \times 10^{52}$	26
080411	1.03	$-1.51^{+0.04}_{-0.05}$	...	259^{+35}_{-27}	$(1.28 \pm 0.16) \times 10^{-5}$	20 - 2000	$9.33^{+1.17}_{-1.17} \times 10^{52}$	27
080413A	2.433	$-1.2^{+0.1}_{-0.1}$	...	170^{+80}_{-40}	5.6 ± 0.2^a	15 - 150	$4.41^{+0.16}_{-0.16} \times 10^{52}$	28,29
080413B	1.1	$-1.23^{+0.25}_{-0.25}$	...	78^{+16}_{-16}	1.4 ± 0.2^a	15 - 150	$1.55^{+0.06}_{-0.06} \times 10^{52}$	1
080603B	2.69	$-1.20^{+0.26}_{-0.32}$	...	200^{+131}_{-59}	$1.51^{+0.4}_{-0.38} \times 10^{-6}$	20 - 1000	$1.11^{+0.29}_{-0.28} \times 10^{53}$	30
080605	1.6398	$-0.87^{+0.13}_{-0.12}$	$-2.58^{+0.31}_{-0.84}$	297^{+46}_{-40}	$(1.6 \pm 0.33) \times 10^{-5}$	20 - 2000	$3.33^{+0.69}_{-0.69} \times 10^{53}$	31

Table 1—Continued

GRB	z	α	β^b	E_p(keV)	Flux(erg/cm^2/s)	Range(keV)	L(erg/s)	Ref.
080607	3.036	$-0.76^{+0.07}_{-0.06}$	$-2.57^{+0.18}_{-0.26}$	348^{+27}_{-27}	$(2.69 \pm 0.54) \times 10^{-5}$	20 - 4000	$2.21^{+0.44}_{-0.44} \times 10^{54}$	32
080721	2.602	$-0.96^{+0.07}_{-0.07}$	$-2.42^{+0.29}_{-0.29}$	497^{+62}_{-62}	$(2.11 \pm 0.35) \times 10^{-5}$	20 - 7000	$1.11^{+0.18}_{-0.18} \times 10^{54}$	1
080804	2.2	$-0.88^{+0.1}_{-0.1}$	...	$315.1^{+67.4}_{-67.4}$	$(7.3 \pm 0.88) \times 10^{-7}$	8 - 35000	$2.86^{+0.34}_{-0.34} \times 10^{52}$	33
080810	3.35	$-1.2^{+0.1}_{-0.1}$	-2.5	580^{+850}_{-263}	$1.7^{+0.1}_{-0.2} \times 10^{-5}$	15 - 1000	$2.39^{+0.14}_{-0.28} \times 10^{54}$	34
080913	6.7	$-0.82^{+0.75}_{-0.53}$	-2.5	121^{+232}_{-39}	$(1.4 \pm 0.058) \times 10^{-6}$	15 - 150	$1.24^{+0.18}_{-0.18} \times 10^{53}$	35,36
080916A	0.689	$-0.99^{+0.05}_{-0.05}$	...	208^{+11}_{-11}	$(4.87 \pm 0.27) \times 10^{-7}$	8 - 35000	$1.08^{+0.06}_{-0.06} \times 10^{51}$	1
081007	0.5295	$-1.4^{+0.4}_{-0.4}$	...	40^{+10}_{-10}	2.2 ± 0.2^a	25 - 900	$4.35^{+0.40}_{-0.40} \times 10^{50}$	1
081008	1.9685	$-0.36^{+0.20}_{-0.20}$	...	$176.4^{+23.9}_{-23.9}$	$(3.21 \pm 0.33) \times 10^{-7}$	8 - 35000	$9.48^{+0.97}_{-0.97} \times 10^{51}$	33
081028	3.038	$0.36^{+0.34}_{-0.34}$	$-2.25^{+0.1}_{-0.1}$	$59.66^{+5.91}_{-5.91}$	$(7.04 \pm 0.65) \times 10^{-7}$	8 - 35000	$4.91^{+0.45}_{-0.45} \times 10^{52}$	33
081118	2.58	$-0.68^{+0.09}_{-0.09}$	...	$98.99^{+5.01}_{-5.01}$	$(6.73 \pm 0.23) \times 10^{-7}$	8 - 35000	$3.99^{+0.14}_{-0.14} \times 10^{52}$	33
081121	2.512	$-0.21^{+0.28}_{-0.28}$	$-1.86^{+0.09}_{-0.09}$	$206.9^{+43.8}_{-43.8}$	$5.16^{+1.53}_{-1.04} \times 10^{-8}$	8 - 35000	$1.38^{+0.22}_{-0.22} \times 10^{53}$	33
081203A	2.1	$-1.29^{+0.15}_{-0.13}$	...	497^{+244}_{-244}	$3.71^{+0.55}_{-0.48} \times 10^{-7}$	15 - 350	$2.63^{+0.39}_{-0.34} \times 10^{52}$	1
081222	2.77	$-0.90^{+0.03}_{-0.03}$	$-2.33^{+0.1}_{-0.1}$	167^{+8}_{-8}	$(1.76 \pm 0.058) \times 10^{-6}$	8 - 35000	$1.01^{+0.03}_{-0.03} \times 10^{53}$	1
090102	1.547	$-0.97^{+0.01}_{-0.01}$	...	461^{+15}_{-15}	$(2.93 \pm 0.091) \times 10^{-6}$	8 - 35000	$4.79^{+0.15}_{-0.15} \times 10^{52}$	1
090424	0.544	$-1.02^{+0.01}_{-0.01}$	$-3.26^{+0.18}_{-0.18}$	$162^{+2.2}_{-2.2}$	$(9.12 \pm 0.14) \times 10^{-6}$	8 - 35000	$1.14^{+0.02}_{-0.02} \times 10^{52}$	1
090429B	9.4	$-0.69^{+0.91}_{-0.76}$	...	$46.21^{+10.66}_{-6.59}$	$1.03^{+0.47}_{-0.32} \times 10^{-7}$	15 - 350	$1.59^{+0.73}_{-0.49} \times 10^{53}$	19
090516	4.109	$-1.03^{+0.26}_{-0.31}$	$-2.1^{+0.1}_{-0.2}$	$51.4^{+20.1}_{-11.4}$	5.3 ± 0.2^a	8 - 1000	$8.70^{+0.33}_{-0.33} \times 10^{52}$	37
090519	3.85	$-0.58^{+0.22}_{-0.22}$	...	$120.5^{+13.8}_{-13.8}$	$(2.25 \pm 0.17) \times 10^{-7}$	8 - 35000	$3.46^{+0.26}_{-0.26} \times 10^{52}$	33
090529	2.625	$-0.75^{+0.03}_{-0.03}$	...	$199.9^{+6.74}_{-6.74}$	$(3.006 \pm 0.063) \times 10^{-6}$	8 - 35000	$1.82^{+0.04}_{-0.04} \times 10^{53}$	33
090618	0.54	$-0.91^{+0.03}_{-0.03}$	$-2.42^{+0.07}_{-0.07}$	$313.2^{+14.0}_{-14.0}$	$(1.73 \pm 0.073) \times 10^{-5}$	8 - 35000	$1.87^{+0.08}_{-0.08} \times 10^{52}$	33
090715B	3	$-1.1^{+0.37}_{-0.37}$	...	134^{+41}_{-41}	$(9 \pm 2.5) \times 10^{-7}$	20 - 2000	$8.78^{+2.44}_{-2.44} \times 10^{52}$	1
090809	2.737	$-0.47^{+0.05}_{-0.05}$	$-2.16^{+0.07}_{-0.07}$	$193.4^{+11.2}_{-11.2}$	$(7.231 \pm 0.6) \times 10^{-6}$	8 - 35000	$3.40^{+0.28}_{-0.28} \times 10^{53}$	33
090812	2.452	$-1.03^{+0.07}_{-0.07}$	...	586^{+192}_{-192}	2.77 ± 0.28^a	100 - 1000	$1.02^{+0.10}_{-0.10} \times 10^{53}$	1
090926B	1.24	$-0.19^{+0.06}_{-0.06}$	...	$95.6^{+1.9}_{-1.9}$	$(4.73 \pm 0.28) \times 10^{-7}$	8 - 35000	$4.46^{+0.26}_{-0.26} \times 10^{51}$	1
090927	1.37	$-0.68^{+0.05}_{-0.05}$	$-2.12^{+0.01}_{-0.01}$	$59.67^{+1.81}_{-1.81}$	$(9.379 \pm 0.23) \times 10^{-6}$	8 - 35000	$9.30^{+0.23}_{-0.23} \times 10^{52}$	33
091018	0.971	$-1.53^{+0.48}_{-0.48}$	...	28^{+13}_{-13}	$(4.32 \pm 0.95) \times 10^{-7}$	20 - 1000	$4.90^{+1.08}_{-1.08} \times 10^{51}$	1
091020	1.71	$-1.20^{+0.06}_{-0.06}$	$-2.29^{+0.18}_{-0.18}$	187^{+25}_{-25}	$(1.88 \pm 0.026) \times 10^{-6}$	8 - 35000	$3.44^{+0.04}_{-0.04} \times 10^{52}$	1
091024	1.092	$-1.5^{+0.4}_{-0.4}$	...	280^{+120}_{-120}	$3.46^{+0.53}_{-0.46} \times 10^{-7}$	15 - 350	$4.08^{+0.62}_{-0.54} \times 10^{51}$	38
091029	2.752	$-1.46^{+0.27}_{-0.27}$	...	$61.4^{+17.5}_{-17.5}$	1.8 ± 0.1^a	15 - 150	$1.40^{+0.08}_{-0.08} \times 10^{52}$	39
091127	0.49	$-0.68^{+0.05}_{-0.05}$	$-2.12^{+0.01}_{-0.01}$	$59.67^{+1.81}_{-1.81}$	$(9.379 \pm 0.23) \times 10^{-6}$	8 - 35000	$7.71^{+0.19}_{-0.19} \times 10^{51}$	33
091208B	1.063	$-1.29^{+0.04}_{-0.04}$	...	119^{+7}_{-7}	$(2.56 \pm 0.097) \times 10^{-6}$	8 - 35000	$1.81^{+0.06}_{-0.06} \times 10^{52}$	1
100425A	1.755	$-0.53^{+2.83}_{-1.46}$	...	< 36.02	$4.74^{+3.46}_{-1.97} \times 10^{-8}$	15 - 350	$< 1.41 \times 10^{51}$	40
100615A	1.398	$-1.24^{+0.08}_{-0.06}$	$-2.27^{+0.11}_{-0.12}$	$85.73^{+7.82}_{-9.33}$	8.3 ± 0.2^a	8 - 1000	$1.06^{+0.03}_{-0.03} \times 10^{52}$	41
100621A	0.542	$-1.70^{+0.13}_{-0.13}$	$-2.45^{+0.15}_{-0.15}$	95^{+15}_{-15}	$(1.7 \pm 0.13) \times 10^{-6}$	20 - 2000	$3.24^{+0.25}_{-0.25} \times 10^{51}$	1
100728A	1.567	$-0.47^{+0.15}_{-0.15}$	$-2.5^{+0.2}_{-0.3}$	390^{+27}_{-25}	$(4.2 \pm 0.7) \times 10^{-6}$	20 - 10000	$6.45^{+1.08}_{-1.08} \times 10^{52}$	42
100728B	2.106	$-0.90^{+0.07}_{-0.07}$	...	130^{+9}_{-9}	$(5.43 \pm 0.35) \times 10^{-7}$	8 - 35000	$1.97^{+0.13}_{-0.13} \times 10^{52}$	1
100814A	1.44	$-0.55^{+0.3}_{-0.3}$	...	147^{+12}_{-10}	$(7.5 \pm 2.5) \times 10^{-7}$	20 - 2000	$1.08^{+0.36}_{-0.36} \times 10^{52}$	43
100816A	0.8049	$-0.31^{+0.05}_{-0.05}$	$-2.77^{+0.17}_{-0.17}$	$136.7^{+4.73}_{-4.73}$	15.59 ± 0.25^a	10 - 1000	$7.38^{+0.12}_{-0.12} \times 10^{51}$	44,45
100906A	1.727	$-1.1^{+0.1}_{-0.1}$	$-2.2^{+0.2}_{-0.3}$	180^{+45}_{-40}	$(2.7 \pm 0.3) \times 10^{-6}$	20 - 2000	$6.90^{+0.77}_{-0.77} \times 10^{52}$	46
101213A	0.414	$-1.1^{+0.07}_{-0.07}$	$-2.35^{+0.29}_{-0.72}$	$309.7^{+48.9}_{-40.0}$	4.67 ± 0.32^a	10 - 1000	$6.32^{+0.43}_{-0.43} \times 10^{50}$	47
101219B	0.55	$-0.33^{+0.36}_{-0.36}$	$-2.12^{+0.12}_{-0.12}$	70^{+8}_{-8}	2.0 ± 0.2^a	10 - 1000	$3.81^{+0.38}_{-0.38} \times 10^{50}$	48
110205A	2.22	$-1.52^{+0.14}_{-0.14}$	...	222^{+74}_{-74}	$(5.1 \pm 0.7) \times 10^{-7}$	20 - 1200	$2.65^{+0.36}_{-0.36} \times 10^{52}$	1
110213A	1.46	$-1.44^{+0.05}_{-0.05}$	...	$98.4^{+8.5}_{-6.9}$	17.7 ± 0.5^a	10 - 1000	$2.23^{+0.06}_{-0.06} \times 10^{52}$	49
110422A	1.77	$-0.53^{+0.17}_{-0.14}$	$-2.65^{+0.28}_{-0.62}$	246^{+37}_{-34}	$(1.2 \pm 0.15) \times 10^{-5}$	20 - 2000	$2.90^{+0.36}_{-0.36} \times 10^{51}$	50
110503A	1.613	$-0.98^{+0.08}_{-0.08}$	$-2.7^{+0.3}_{-0.3}$	219^{+19}_{-19}	$(10 \pm 1) \times 10^{-6}$	20 - 5000	$1.89^{+0.19}_{-0.19} \times 10^{53}$	1
110715A	0.82	$-1.23^{+0.09}_{-0.08}$	$-2.7^{+0.2}_{-0.5}$	120^{+12}_{-11}	$(1.1 \pm 0.1) \times 10^{-5}$	20 - 10000	$4.31^{+0.39}_{-0.39} \times 10^{52}$	51

Table 1—Continued

GRB	z	α	β^b	E_p(keV)	Flux(erg/cm^2/s)	Range(keV)	L(erg/s)	Ref.
110731A	2.83	$-0.8^{+0.03}_{-0.03}$	$-2.98^{+0.3}_{-0.3}$	304^{+13}_{-13}	20.9 ± 0.5^a	10 - 1000	$3.06^{+0.07}_{-0.07} \times 10^{53}$	52
110801A	1.858	$-1.7^{+0.12}_{-0.15}$	-2.5	140^{+1270}_{-50}	$8.91^{+1.68}_{-1.4} \times 10^{-8}$	15 - 350	$4.43^{+0.84}_{-0.70} \times 10^{51}$	53
110808A	1.348	$-1.07^{+0.12}_{-0.11}$	...	4238^{+3270}_{-1530}	$(1.1 \pm 0.2) \times 10^{-4}$	20 - 10000	$8.96^{+1.63}_{-1.63} \times 10^{53}$	54
110818A	3.36	$-1.33^{+0.08}_{-0.08}$	...	$256.3^{+55.3}_{-55.3}$	5.0 ± 1.4^a	10 - 1000	$7.23^{+2.03}_{-2.03} \times 10^{52}$	55
111008A	4.9898	$-1.36^{+0.24}_{-0.21}$	...	149^{+52}_{-28}	$(1.4 \pm 0.3) \times 10^{-6}$	20 - 2000	$4.95^{+1.06}_{-1.06} \times 10^{53}$	56
111107A	2.893	$-1.38^{+0.21}_{-0.21}$	...	108^{+32}_{-32}	2.6 ± 0.3^a	10 - 1000	$1.81^{+0.21}_{-0.21} \times 10^{52}$	57
111123A	3.1516	$-1.30^{+0.26}_{-0.24}$	...	$107.79^{+125.38}_{-25.03}$	$7.89^{+1.1}_{-0.89} \times 10^{-8}$	15 - 350	$9.80^{+1.37}_{-1.11} \times 10^{51}$	40
111228A	0.714	$-1.9^{+0.1}_{-0.1}$	$-2.7^{+0.3}_{-0.3}$	34^{+3}_{-3}	27 ± 1^a	10 - 1000	$6.67^{+0.25}_{-0.25} \times 10^{51}$	58
120119A	1.728	$-0.98^{+0.03}_{-0.03}$	$-2.36^{+0.09}_{-0.09}$	$189.2^{+8.3}_{-8.3}$	16.86 ± 0.39^a	10 - 1000	$5.98^{+0.14}_{-0.14} \times 10^{52}$	59
120326A	1.798	$-0.98^{+0.14}_{-0.14}$	$-2.53^{+0.15}_{-0.15}$	$46.45^{+3.67}_{-3.67}$	3.1 ± 0.05^a	10 - 1000	$5.91^{+0.10}_{-0.10} \times 10^{51}$	60
120327A	2.813	$-1.14^{+0.26}_{-0.28}$	...	$106.09^{+80.1}_{-22.76}$	$3.88^{+0.65}_{-0.52} \times 10^{-7}$	15 - 350	$3.42^{+0.57}_{-0.46} \times 10^{52}$	40
120712A	4.1745	$-0.6^{+0.2}_{-0.2}$	$-1.8^{+0.2}_{-0.2}$	124^{+26}_{-26}	3.5 ± 0.2^a	10 - 1000	$1.35^{+0.08}_{-0.08} \times 10^{53}$	61
120714B	0.3984	$-0.29^{+0.96}_{-0.8}$	...	$60.8^{+25.92}_{-10.22}$	$1.8^{+1.13}_{-0.68} \times 10^{-8}$	15 - 350	$1.15^{+0.72}_{-0.44} \times 10^{49}$	40
120724A	1.48	$-0.75^{+2.34}_{-1.23}$	...	< 31.9	$1.95^{+1.58}_{-0.87} \times 10^{-8}$	15 - 350	$< 4.19 \times 10^{50}$	40
120802A	3.796	$-0.96^{+0.60}_{-0.53}$	...	$52.96^{+12.58}_{-6.84}$	$1.85^{+0.34}_{-0.27} \times 10^{-7}$	15 - 350	$3.51^{+0.65}_{-0.51} \times 10^{52}$	40
120811C	2.671	$-1.19^{+0.32}_{-0.30}$	...	$46.26^{+4.32}_{-4.14}$	$2.47^{+0.25}_{-0.22} \times 10^{-7}$	15 - 350	$2.23^{+0.23}_{-0.20} \times 10^{52}$	40
120907A	0.97	$-0.75^{+0.25}_{-0.25}$	...	$154.5^{+32.9}_{-32.9}$	4.3 ± 0.4^a	10 - 1000	$2.53^{+0.24}_{-0.24} \times 10^{51}$	62
120909A	3.93	$-1.3^{+0.1}_{-0.1}$	...	370^{+140}_{-140}	3.0 ± 0.2^a	10 - 1000	$7.65^{+0.51}_{-0.51} \times 10^{52}$	63
120922A	3.1	$-1.6^{+0.7}_{-0.7}$	$-2.3^{+0.1}_{-0.1}$	$37.7^{+3.5}_{-3.5}$	3.4 ± 0.3^a	10 - 1000	$3.02^{+0.27}_{-0.27} \times 10^{52}$	64
121027A	1.77	$-1.49^{+0.43}_{-0.39}$	...	$61.75^{+437.65}_{-13.25}$	$8.34^{+2.24}_{-1.64} \times 10^{-8}$	15 - 350	$2.92^{+0.79}_{-0.57} \times 10^{53}$	40
121128A	2.2	$-0.80^{+0.12}_{-0.12}$	$-2.41^{+0.1}_{-0.1}$	$62.2^{+4.6}_{-4.6}$	17.9 ± 0.5^a	10 - 1000	$6.67^{+0.19}_{-0.19} \times 10^{52}$	65
121211A	1.023	$-0.3^{+0.34}_{-0.34}$	...	$95.96^{+12.6}_{-12.6}$	2.402 ± 0.202^a	10 - 1000	$1.25^{+0.11}_{-0.11} \times 10^{51}$	66
130215A	0.597	$-1^{+0.2}_{-0.2}$	$-1.6^{+0.03}_{-0.03}$	155^{+63}_{-63}	3.5 ± 0.3^a	10 - 1000	$2.16^{+0.18}_{-0.18} \times 10^{51}$	67
130408A	3.758	$-0.7^{+0.15}_{-0.15}$	$-2.3^{+0.3}_{-0.3}$	272^{+40}_{-40}	$(5.2 \pm 0.5) \times 10^{-6}$	20 - 10000	$6.12^{+0.59}_{-0.59} \times 10^{53}$	68
130420A	1.297	$-1^{+0.13}_{-0.13}$	...	56^{+3}_{-3}	5.2 ± 0.4^a	10 - 1000	$3.65^{+0.28}_{-0.28} \times 10^{51}$	69
130427A	0.3399	$-0.789^{+0.003}_{-0.003}$	$-3.06^{+0.02}_{-0.02}$	830^{+5}_{-5}	1052 ± 2^a	8 - 1000	$1.90^{+0.00}_{-0.00} \times 10^{53}$	70
130505A	2.27	$-0.31^{+0.09}_{-0.09}$	$-2.26^{+0.07}_{-0.07}$	604^{+49}_{-49}	$(6.9 \pm 0.3) \times 10^{-5}$	20 - 1200	$3.98^{+0.17}_{-0.17} \times 10^{54}$	71
130514A	3.6	$-1.44^{+0.17}_{-0.15}$	...	110^{+42}_{-21}	$2.06^{+0.23}_{-0.18} \times 10^{-7}$	15 - 350	$3.82^{+0.43}_{-0.33} \times 10^{52}$	72
130606A	5.913	$-1.14^{+0.15}_{-0.15}$	...	294^{+90}_{-50}	$3.15^{+0.56}_{-0.46} \times 10^{-7}$	15 - 350	$2.04^{+0.36}_{-0.30} \times 10^{53}$	73
130610A	2.092	$-1^{+0.1}_{-0.1}$	...	$294.9^{+42.9}_{-42.9}$	4.5 ± 0.9^a	10 - 1000	$2.55^{+0.51}_{-0.51} \times 10^{52}$	74
130612A	2.006	$-1.3^{+0.3}_{-0.3}$	...	$61.9^{+10.5}_{-10.5}$	4.1 ± 0.2^a	10 - 1000	$9.48^{+0.46}_{-0.46} \times 10^{51}$	75
130701A	1.155	$-1.1^{+0.1}_{-0.1}$	...	89^{+4}_{-4}	$(4.3 \pm 0.4) \times 10^{-6}$	20 - 10000	$4.27^{+0.40}_{-0.40} \times 10^{52}$	76
130831A	0.4791	$-1.51^{+0.1}_{-0.1}$	$-2.8^{+0.1}_{-0.1}$	67^{+4}_{-4}	$(2.6 \pm 0.3) \times 10^{-6}$	20 - 10000	$3.42^{+0.39}_{-0.39} \times 10^{51}$	77
130907A	1.238	$-0.65^{+0.03}_{-0.03}$	$-2.22^{+0.05}_{-0.05}$	390^{+16}_{-16}	$(2.2 \pm 0.1) \times 10^{-5}$	20 - 10000	$1.82^{+0.08}_{-0.08} \times 10^{53}$	78
131030A	1.295	$-0.71^{+0.12}_{-0.12}$	$-2.95^{+0.28}_{-0.28}$	177^{+10}_{-10}	$(10 \pm 1) \times 10^{-6}$	20 - 10000	$1.08^{+0.11}_{-0.11} \times 10^{53}$	79

Notes: [a] For these GRBs, the peak flux is in units of photons cm^{-2} s^{-1}.

[b] For those GRBs with β value, the spectra are described well by Band model. But for the GRBs without β value, the spectra are described by power-low with an exponential cutoff model.

Reference:[1]Nava et al. (2012), [2]Golenetskii et al. (2005a), [3]Golenetskii et al. (2005b), [4]Sugita et al. (2009), [5]Butler et al. (2007), [6]Golenetskii et al. (2005c), [7]Barbier et al. (2006), [8]Golenetskii et al. (2006a), [9]Sakamoto et al. (2006), [10]Golenetskii et al. (2006b), [11]Stamatikos et al. (2006), [12]Golenetskii et al. (2006c), [13]Golenetskii et al. (2006d), [14]Golenetskii et al. (2006e), [15]Golenetskii et al. (2006f), [16]Golenetskii et al. (2007a), [17]Ohno et al. (2007), [18]Barbier et al. (2007), [19]Butler et al. (2010), [20]Golenetskii et al. (2007b), [21]Golenetskii et al. (2007c), [22]Golenetskii et al. (2007d), [23]Golenetskii et al. (2007e), [24]Golenetskii et al. (2007f), [25]Stamatikos et al. (2008), [26]Golenetskii et al. (2008a), [27]Golenetskii et al. (2008b), [28]Tueller et al. (2008), [29]Ohno et al. (2008), [30]Golenetskii et al. (2008c), [31]Golenetskii et al. (2008d), [32]Golenetskii et al. (2008e), [33]Nava et al. (2011), [34]Sakamoto et al. (2008), [35]Pal'Shin et al. (2008), [36]Greiner et al. (2009), [37]McBreen (2009), [38]Golenetskii et al. (2009), [39]Barthelmy et al. (2009), [40]Butler's website[1] & *Swift* official website[2]. [41]Foley & Briggs (2010), [42]Golenetskii et al. (2010a), [43]Golenetskii et al. (2010b), [44]Fitzpatrick (2010a), [45]Fitzpatrick (2010b), [46]Golenetskii et al. (2010c), [47]Gruber (2010), [48]van der Horst (2010), [49]Foley (2011), [50]Golenetskii et al. (2011a), [51]Golenetskii et al. (2011b), [52]Golenetskii et al. (2011c), [53]Sakamoto et al. (2011), [54]Golenetskii et al. (2011d), [55]Xiong (2011), [56]Golenetskii et al. (2011e), [57]Pelassa (2011), [58]Briggs & Younes (2011), [59]Gruber (2012a), [60]Collazzi (2012), [61]Gruber (2012b), [62]Younes & Barthelmy (2012), [63]Chaplin (2012), [64]Younes (2012), [65]McGlynn (2012), [66]Yu (2012), [67]Younes & Bhat (2013), [68]Golenetskii et al. (2013a), [69]Xiong & Rau (2013), [70]von Kienlin (2013), [71]Golenetskii et al. (2013b), [72]Pal'Shin et al. (2013), [73]Barthelmy et al. (2013), [74]Fitzpatrick & Pelassa (2013), [75]Fitzpatrick (2013), [76]Golenetskii et al. (2013c), [77]Golenetskii et al. (2013d), [78]Golenetskii et al. (2013e), [79]Golenetskii et al. (2013f).

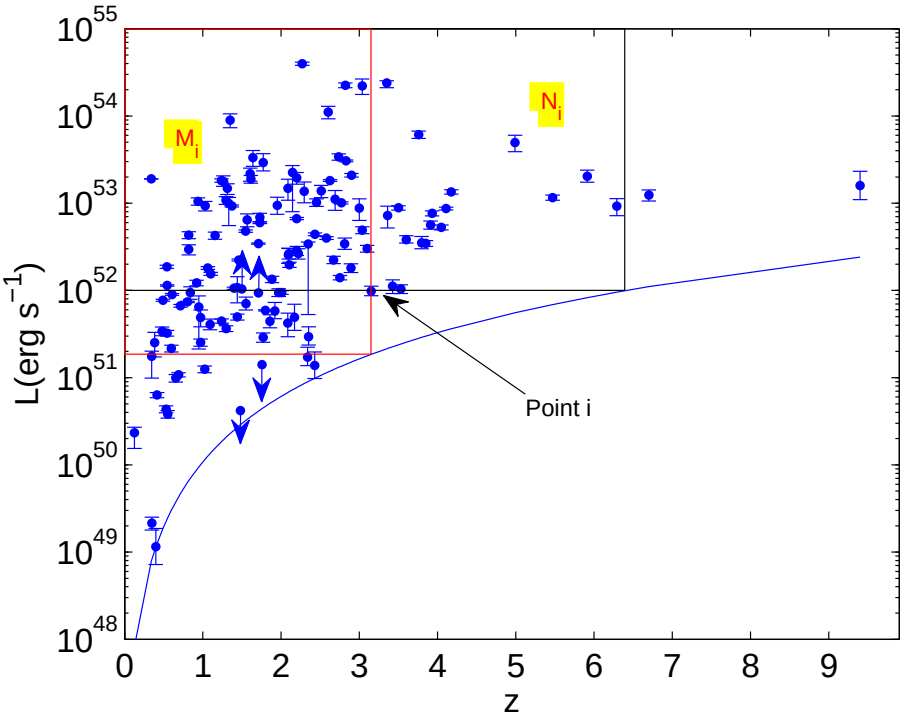

Fig. 1.— The luminosity distribution of 127 GRBs after K-correction. The blue dots represent GRBs and the blue line represents observational limit of *Swift*. We take the flux limit as 2.0×10^{-8} erg cm^{-2} s^{-1}. M_i and N_i are also shown. The error bars are 1σ errors.

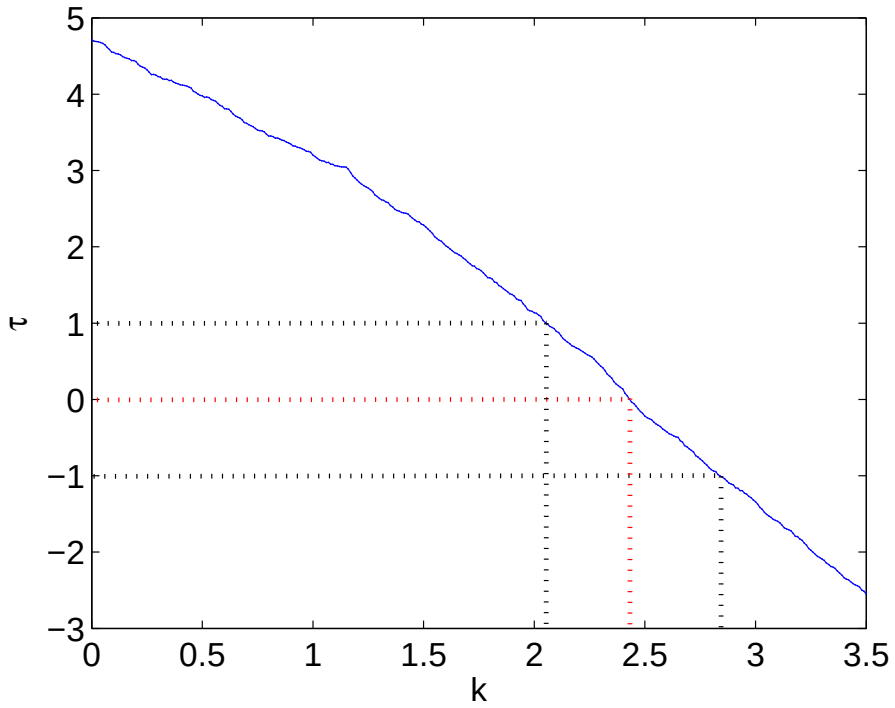

Fig. 2.— The value of test statistic τ as a function of k. The red dotted line represents the best fit for $\tau = 0$, and the black dotted lines are 1σ errors. The value of k is $k = 2.43^{+0.41}_{-0.38}$ at 1σ confidence level. It also shows that $\tau = 4.7$ when $k = 0$, which means $k = 0$ is excluded at 4.7σ confidence level.

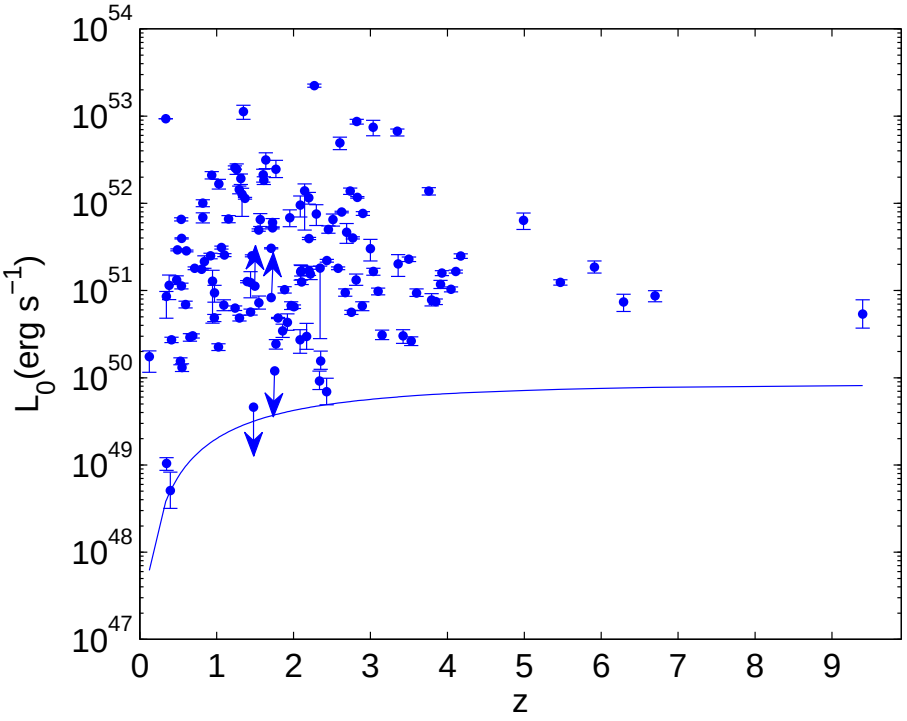

Fig. 3.— The non-evolving luminosity $L_0 = L/(1+z)^{2.43}$ of 127 GRBs above the truncation line. The blue line represents observational limit. The error bars are 1σ errors.

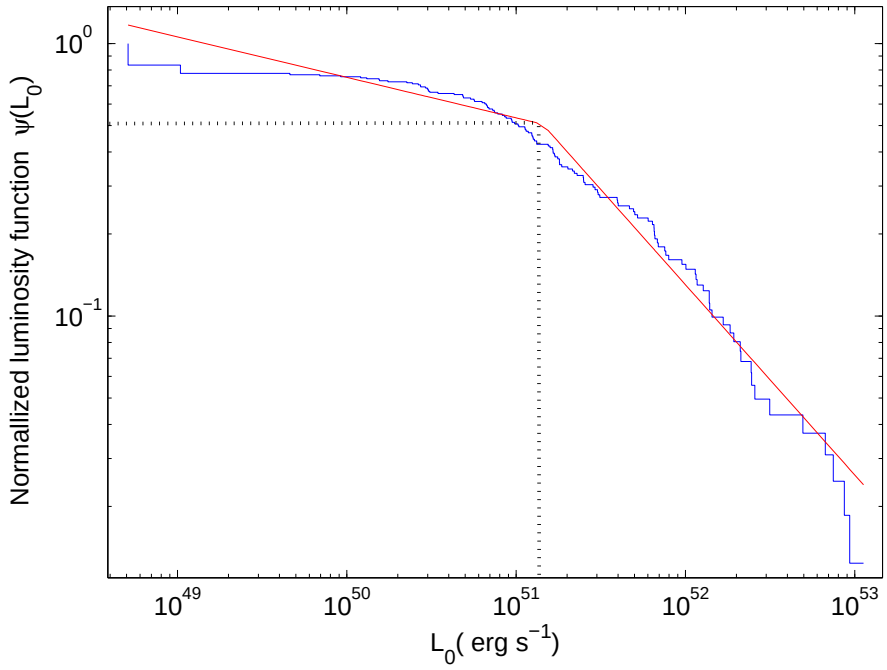

Fig. 4.— The cumulative luminosity function $\psi(L_0)$, which is normalized to unity at the lowest luminosity. The red line is the best fit with a broken power law model. The luminosity function can be expressed as $\psi(L_0) \propto L_0^{-0.14\pm0.02}$ for dim GRBs and $\psi(L_0) \propto L_0^{-0.70\pm0.03}$ for bright GRBs, with the break point $L_0^b = 1.43 \times 10^{51}$ erg s^{-1}.

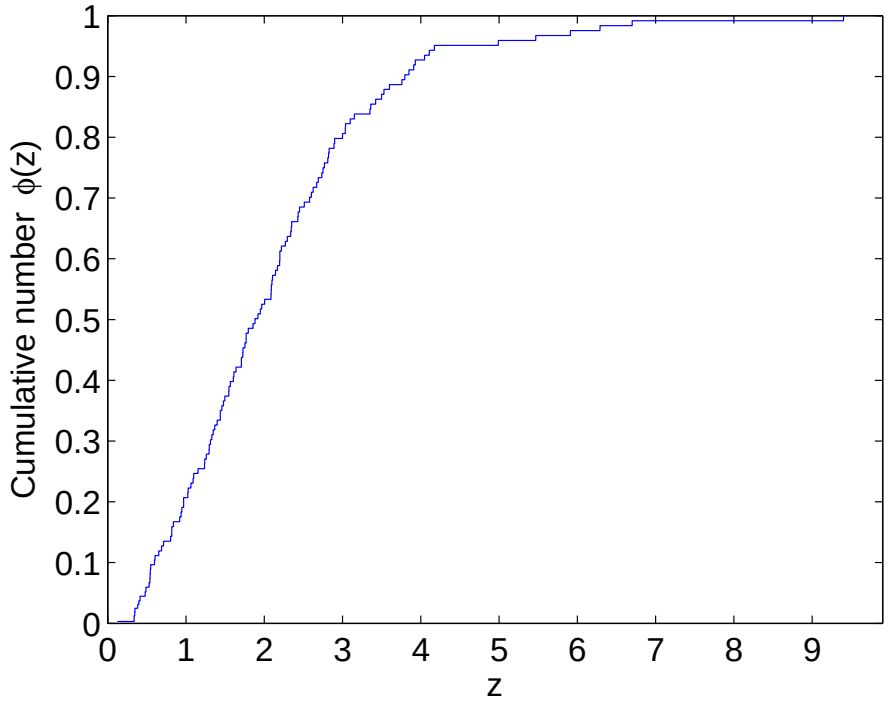

Fig. 5.— The normalized cumulative redshift distribution of GRBs.

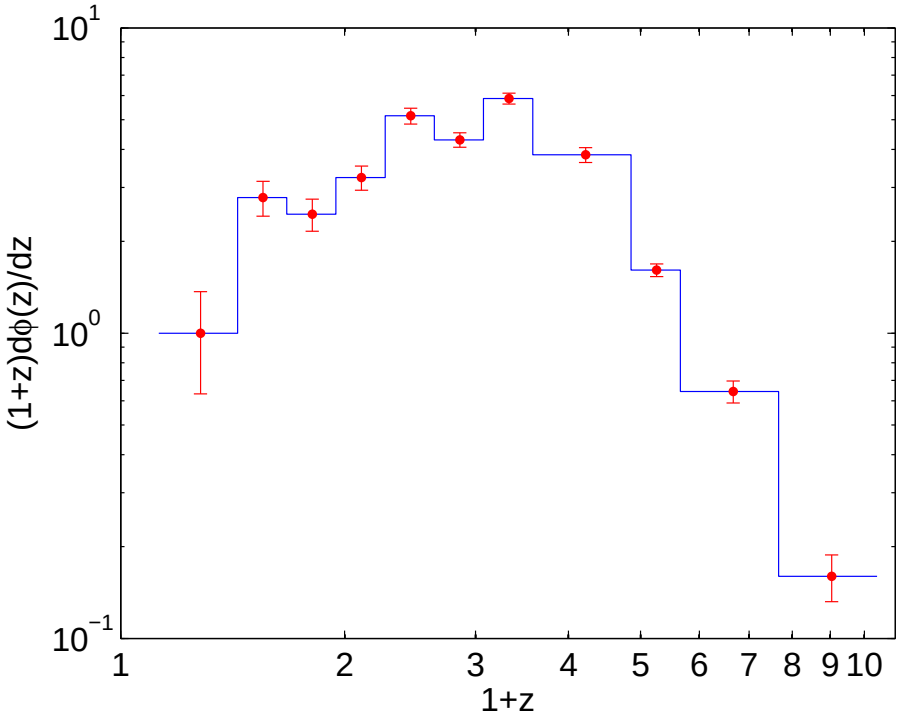

Fig. 6.— The evolution of $(1+z)\frac{d\phi(z)}{dz}$ as function of redshift z with 1σ errors, which is normalized to unity at the first point.

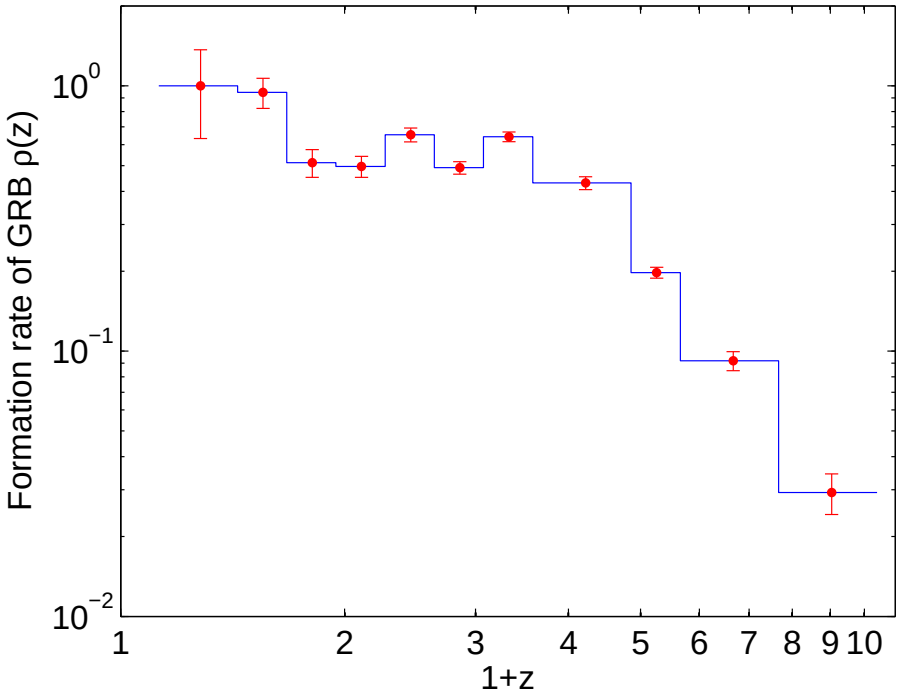

Fig. 7.— The comoving formation rate $\rho(z)$ of GRBs, which is normalized to unity at the first point. The 1σ error is also shown.

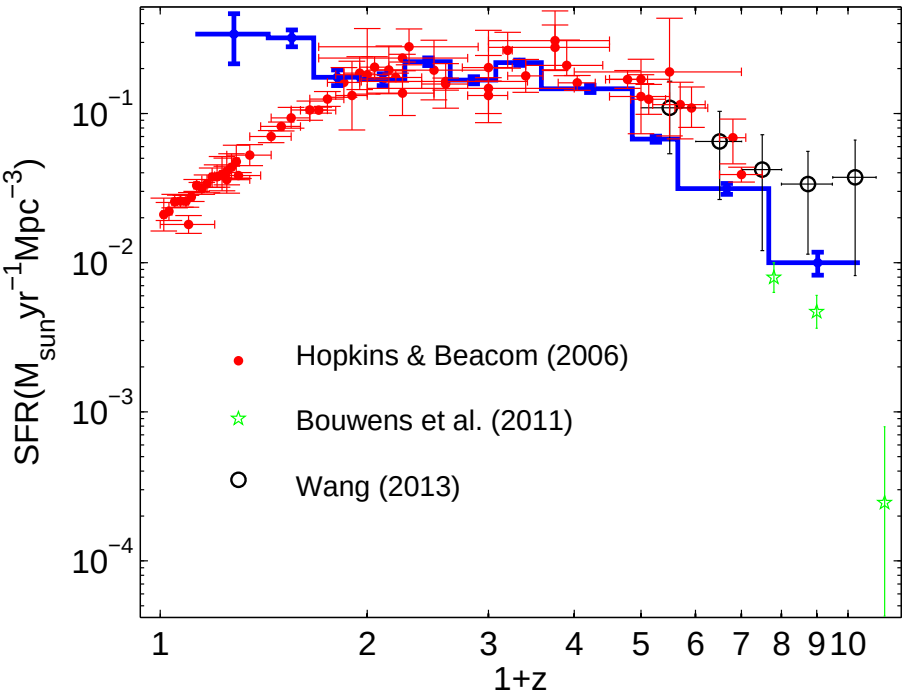

Fig. 8.— The comparison between GRB formation rate $\rho(z)$ (blue) and the observed SFR. The SFR data are taken from Hopkins & Beacom (2006), which are shown as red dots. The SFR data from Bouwens et al. (2011) (stars) and Wang (2013) (open circles) are also used. All error bars are 1σ errors.

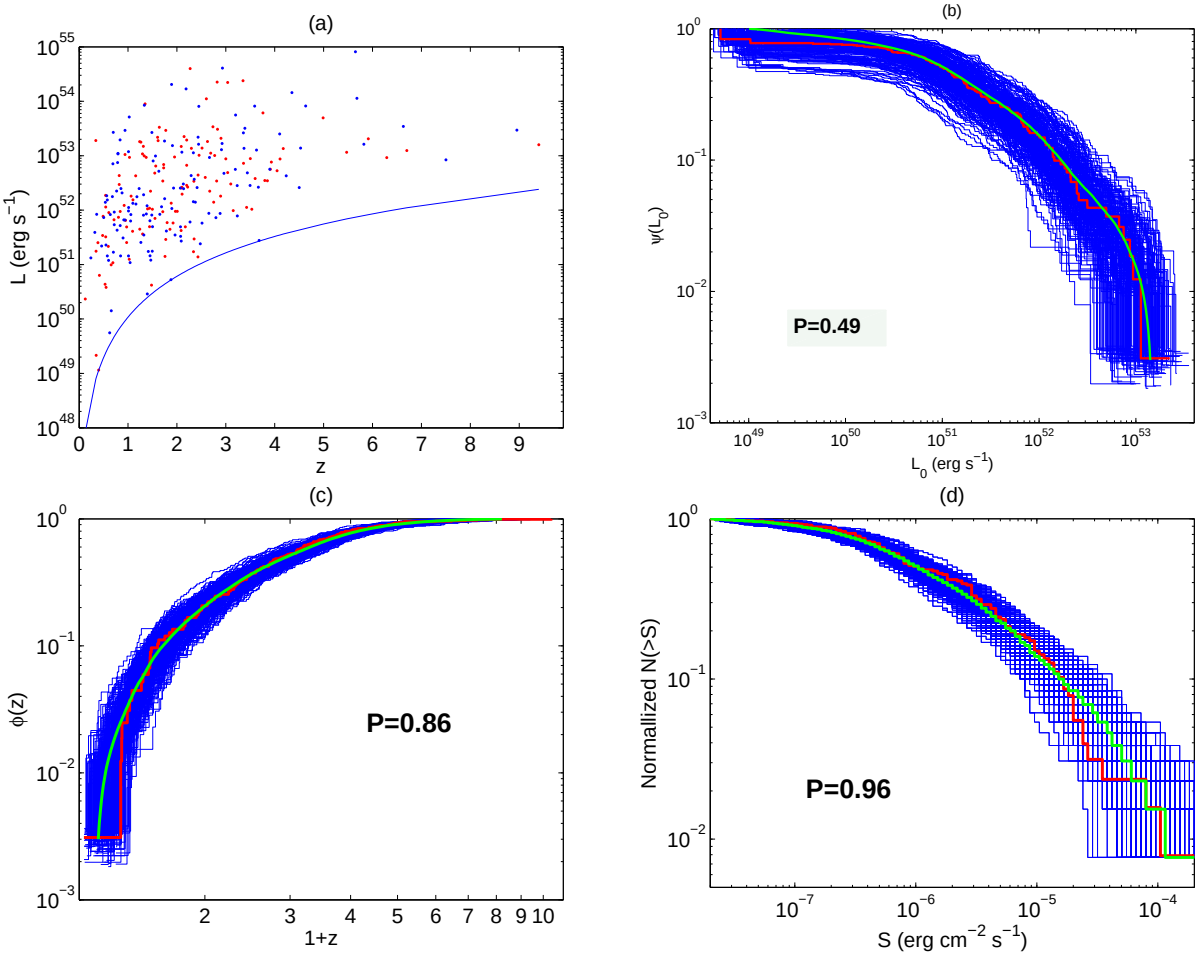

Fig. 9.— The comparison of the simulated data (blue) and the observed data (red). These four panels show luminosity-redshift distribution, cumulative luminosity function, cumulative number distribution and $\log N - \log S$ distribution respectively. For panel (a), we choose one sample from the 200 simulated samples randomly. For other panels (b), (c) and (d), the green curves represent the mean distribution of those 200 simulated samples. The chance probabilities of Kolmogorov-Smirnov tests between the distributions of observed data and the mean distributions of the simulated data are also presented.

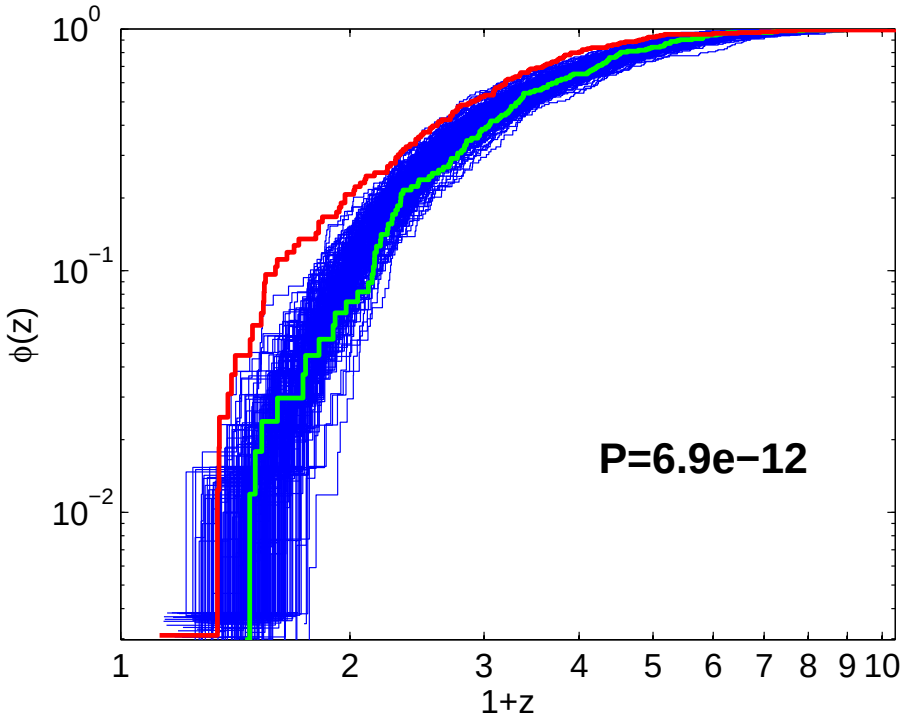

Fig. 10.— The comparison between the cumulative redshift distributions of simulated data (blue) and observed data (red). The mean distribution of the 200 simulated samples is given by green curve. In this case we use the SFR from Yüksel et al. (2008). The chance probability of the Kolmogorov-Smirnov test between the observed data and the simulated data is $p = 6.9 \times 10^{-12}$, from which the observed data and the simulated data from the same sample can be discarded.